Reliability Engineering and System Safety 239 (2023) 109531

Contents lists available at ScienceDirect

Reliability Engineering and System Safety

journal homepage: www.elsevier.com/locate/ress

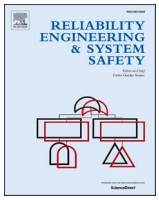

The influence of model and measurement uncertainties on damage detection of experimental structures through recursive algorithms

Mehrdad Ebrahimi [a], Elnaz Nobahar [a], Reza Karami Mohammadi [a], Ehsan Noroozinejad Farsangi [b,*], Mohammad Noori [c,d], Shaofan Li [e]

[a] Department of Civil Engineering, K.N. Toosi University of Technology, Tehran, Iran
[b] Urban Transformations Research Centre (UTRC), Western Sydney University, NSW, Australia
[c] Department of Mechanical Engineering, California Polytechnic State University, San Luis Obispo, CA, United States of America
[d] School of Civil Engineering, University of Leeds, Leeds LS2 9JT, UK
[e] Department of Civil and Environmental Engineering, University of California, Berkeley, CA, United States of America

ARTICLE INFO

Keywords:
Uncertainty
Extended Kalman filter
Unscented Kalman filter
Recursive algorithms
Damage detection
Information entropy
Sensors

ABSTRACT

In this work, we developed a framework for identifying frame-type structures regarding the measurement uncertainty and the uncertainty involved in inherent and structural parameters. The identification process is illustrated and examined on a one-eight-scale four-story moment-resisting steel frame under seismic excitation using two well-known recursive schemes: the Extended Kalman filter (EKF) and Unscented Kalman Filter (UKF) methods. The nonlinear system equations were assessed by applying a first-order instantaneous linearization approach through the EKF method. In contrast, the UKF algorithm employs several sample points to estimate moments of random variables' nonlinear transformations. A nonlinear transformation is applied to distribute sample points to derive the precise mean and covariance up to the second order of any nonlinearity. Accordingly, it is theoretically expected that the UKF algorithm is more capable of identifying the nonlinear systems and determining the unknown parameters than the EKF algorithm. The capability of the EKF and UKF algorithms was assessed by considering a 4-story moment-resisting steel frame with several inherent uncertainties, including the material behavior model, boundary conditions, and constraints. In addition to these uncertainties, the combination of acceleration and displacement responses of different structural levels is employed to evaluate the capability of the algorithms. The information entropy measure is used to investigate further the uncertainty of a group of established model parameters. As highlighted, a good agreement is observed between the results using the information entropy measure criterion and those using the UKF and EKF algorithms. The results illustrate that using the responses of fewer levels placed in the proper positions may lead to improved outcomes than those of more improperly positioned levels.

1. Introduction

Before building any structure, random technique models are typically used to represent all the potential uncertainties related to the system parameters [1]. During this phase, the safety of the structural systems is quantified through the concept of probability of failure or reliability index. After building structural systems and measuring their responses under various types of excitations, it is possible to evaluate their states, such as the damage extension and their remaining lifetime, through system identification methods. Thus, robust interpretation of measurement data increases the safety and reliability of the built environment. Over the last decades, structural system identification approaches using both ambient vibrations with low amplitude and forced vibrations with high amplitude have been extensively studied for health monitoring and damage detection [2–6]. Regardless of identifying structural systems using measured input-output or output-only data, these approaches can be categorized into time-domain, frequency-domain, time-frequency, modal, black-box, structural model updating techniques, and methods that circumvent nonlinearity utilizing linearization [7]. Structural model updating is a well-established method of significant concern to many researchers. According to this method, a finite element (FE) model is updated using iterative or

* Corresponding author.
E-mail address: ehsan.noroozinejad@westernsydney.edu.au (E. Noroozinejad Farsangi).

https://doi.org/10.1016/j.ress.2023.109531
Received 10 January 2023; Received in revised form 23 July 2023; Accepted 25 July 2023
Available online 28 July 2023

non-iterative procedures by adjusting various parameters to minimize the discrepancy between the response of the baseline structure and that of the FE model [8]. Developing structural models, especially those with high complexities, involves difficulties because of considering several modeling assumptions and uncertainties [9]. These challenges are due to structural geometric nonlinearity, element nonlinearity, material nonlinearity, and boundary conditions, which sometimes are addressed by reducing the model to the most significant parameters [10,11]. On the other hand, uncertainty assessment and reliability estimation are the essential features of structural model updating. These features play crucial functions in controlling the reliability of updated models. In this respect, an effective evaluation of complicated uncertainty components of structural systems is required for predicting their exact behavior under dynamic situations. However, there is a notable absence of investigation on uncertainties for dynamic systems under forced vibrations [12].

Regardless of any source of uncertainty, FE model updating (FEMU) procedures have been studied in linear and nonlinear frameworks. As the name suggests, the structure has been assumed to behave linearly before and after damage states for linear categories. This method evaluates the identification of the structural characteristics by establishing the difference between the modal or extracted characteristics of the baseline and FE models. However, the linear FEMU method is ineffective for some reasons. For instance, it cannot identify minor structural damages, which have negligible effects on the overall characteristics of the structure. Also, it assumes a linearly elastic behavior for the structure in the range of infinitesimal deformations. Therefore, employing nonlinear FE model updating techniques has been considered an integral part of FE methods, attracting the attention of several researchers [13–15]. From another perspective, the structural system identification approaches can also be classified into offline (batch estimation) and online (or recursive) techniques [16]. The data size is constant for offline approaches as they rely on iterative methods. Both approaches take advantage of accessible data, except that online approaches use the data as it becomes available [17]. Concerning the recursive methods, several approaches have been recommended in favor of the nonlinear FEMU and evaluating the structural parameters. Some of these techniques are the Recursive autoregressive and moving average with exogenous input (ARMAX) [18], the recursive Least Square (RLS) [19,20], particle filter (PF) [21,22], Bayesian inference (BI) [23,24], and Kalman Filter (KF) [25,26]. Among these methods, the KF and its several versions have been effectively implemented for real-time linear model calibration. The KF method can estimate the system's state by incorporating several factors, including the dynamic response equations of the system, noisy input data, and the noisy output response of the system. However, the KF technique has not been directly implemented for nonlinear systems with a nonlinear system state or nonlinear measurement equations [27–32]. Extended Kalman Filter (EKF) is another version of the KF offered in the literature to address nonlinear problems [33–37]. This method uses a first-order Taylor series approximation to linearize the nonlinear model near the best-estimated state. Afterward, the obtained post-estimate at every individual time step is used as the center point for the next step of the linearization by applying the KF prediction-correction technique to the linearized system.

In the case of a nonlinear system with high degrees of nonlinearities, the linearization may cause several errors, thereby limiting the application of this method for highly nonlinear systems. To address this drawback, Julier et al. proposed another version of KF methods, namely the Unscented Kalman Filter (UKF) [38,39]. In contrast to the EKF, which employs the first-order instantaneous linearization technique for assessing the nonlinear system equations, the UKF uses a deterministic sampling method with quite a few sample points for estimating the probability density through a Gaussian density function. The real value of mean and covariance up to the second-order of any nonlinearity have been obtained through a nonlinear transformation's distribution of sample points. Consequently, as theoretically hypothesized, the UKF has better estimation than EKF regarding problems with higher-order nonlinearities. In this respect, several research studies have applied these methods for nonlinear state estimation and parameter identification of various systems [40]. To examine the capability of the EKF and UKF methods, Wu and Smyth [41] developed a comparative study of a single degree of freedom nonlinear system with a Bouc-Wen-Baber-Noori (BWBN) hysteretic [42,43] restoring force element, a two-degree of freedom linear structural system, and a two-degree of freedom nonlinear elastic system, under the Chi-Chi earthquake excitation. Lin and Zhang [44] examined the capability of the EKF method in assessing the parameters of a single-degree-of-freedom system with a BWBN hysteretic restoring force under a simulated ground motion excitation. In addition, Chatzi and Smyth compared the UKF and Particle Filter (PF) of a three-degree of freedom system with a BWBN hysteresis model [21].

Diaz et al. [45] proposed an approach based on the integration of UKF and Constitutive Relation Error Observer for structural health monitoring (SHM) of gradually degraded reinforced concrete (RC) structures tested on a shake table. Notably, most of the relevant research has focused on simple structures, including the one- or multi-degrees of freedom mass-spring-dashpot systems. Besides, the material constitutive models or force-deformation behavior models considered in these studies include linear elastic, nonlinear elastic, bilinear, and Bouc-Wen [46,47] restoring force models lacking adequate precision or details. Besides, the employed models have no physical significance for extracting the behavior of real complex structures. Recently, Astroza et al. [48] conducted a nonlinear FE simulation on a column of a concrete bridge and a 3-story SAC structure using the UKF method to assess the time-invariant parameters of the material model.

Despite various applications of these algorithms in structural system identification, it suffers some shortcomings: Lack of implementation in calibrating real structures. This issue involves several complexities and uncertainties, such as complicated components, improper boundary conditions, and incompatible behavior of material models. Engineering models are known to be approximate exhibitions of actuality. When inexact models are engaged in the design, health monitoring, and damage detection, it is usually more reasonable when they are partially conservative rather than the contrary. The vast literature on this subject reveals no general technique for clustering if a model is conservative or not and how conservative it is. Hence, there is a considerable lack of study on uncertainties in system identification and damage detection of real-world systems [49–52].

The intrinsic uncertainties and modeling errors will induce errors between a system's real response and desirable response, resulting in a response reliability problem. Liu et al. [53] presented an approach to investigate the effect of mixed uncertain parameters like randomness in the structural dynamic analysis model. Mi et al. [54] investigated the reliability analysis of complicated systems with typical damages and complex uncertainties. In another study, Xu et al. [55] studied the uncertainty of the damaged elements of crucial infrastructure systems through numerical experiments on different models. Thapa and Missoum [56] proposed a methodology for uncertainty quantification of composite wind turbine blades. To this end, they incorporated the diversity in material and geometric parameters and loading conditions under modal, failure, and buckling analyses. Hao et al. [57] established a framework to analyze uncertainty effects on the probability of failure of composite shell structures. Vishwanath and Banerjee [58] examined uncertainties from various sources, such as the corrosion action, material parameters variety, and primary cracks on the concrete elements on gradual degradation and seismic susceptibility of reinforced concrete (RC) bridge piers. Zheng et al. [59] examined uncertainties in the unknown model parameters of dynamic excitations arising from different sources on the precision of produced demand of tall buildings. Elsewhere, Li et al. [60] presented a methodology that captures the influence of soil spatial variation and ground motion uncertainties at different supports on the seismic behavior of large-span cable-stayed bridges.

According to the above literature review, it can be concluded that

accuracy is the priority among the essential characteristics of a system identification framework. The present study applies EKF and UKF algorithms to experimentally examine the modeling error and uncertainties of a 1:8-scale frame on an earthquake simulator facility at the University of New York at Buffalo (SUNY-NEES). The efficacy of various uncertainties on the capabilities of EKF and UKF was studied by incorporating BWBN [42,43] and Giuffre-Manegoto-pinto (G-M-P) models in all section fibers, followed by using the acceleration and displacement responses of all stories of the structure, and their combination, under seismic ground motions.

As highlighted in the references [61,62], one of the uncertainties affecting the operation of damage detection of a structure is the quality and the quantity measures for selecting the collected data. These factors mainly rely on the location, type, and number of measuring sensors. The results show that some measured input data have a higher impact on the calibration of the structural responses, and the calibrated structural models contain fewer errors. Thus, following the structural system identification method to investigate which level of the structure and response type leads to better estimation and identification, the information entropy measure (IEM) approach can be utilized. The optimal sensor location can be evaluated by the direct use of the minimized IEM approach in estimating the parameters of the model. Therefore, the information entropy criterion is implemented, the model is updated via finite element analysis, and various responses of different test frame levels are employed to identify the best location to position the sensors in the structure. Overall, comparing the results of the FE analyses and the random selection of sensor locations indicates a close match between them. A brief review of the application of the EKF and UKF methods and the IEM criterion is then discussed. Subsequently, the overall characteristics of the steel structure are presented. Finally, the details of the modeling and different material behavior models are developed, the results are interpreted, and conclusions are drawn.

2. Kalman filter

The general discrete-time state-space expression for systems can be described according to the following equation:

$$x_{k+1} = f_k(x_k, u_k) + w_k \tag{1}$$

$$y_{k+1} = g_{k+1}(x_{k+1}, u_{k+1}) + v_{k+1} \tag{2}$$

where x_k, u_k, and y_k account for the state vector, input vector, and measurement vector, respectively, at $t_k = k\Delta t$. Here, Δt is the time interval. Also, w_k is the process noise due to the unmeasured random disturbances of the existing system and v_{k+1} is the measurement noise. The $w_k \sim N(0, Q_k)$ and $v_k \sim N(0, R_k)$ are the independent Gaussian white noise with zero median and covariance matrices of Q_k and R_k, respectively. The f_k and g_{k+1} functions are respectively employed to correlate the current state (x_k) and the next state (x_{k+1}), as well as the next state (x_{k+1}) and the next measurement (y_{k+1}). For linear systems, Eqs. (1) and (2) can be simplified as follows:

$$x_{k+1} = A_k x_k + B_k u_k + w_k \tag{3}$$

$$y_{k+1} = C_{k+1} x_{k+1} + D_{k+1} u_{k+1} + v_{k+1} \tag{4}$$

In these equations, A_k, B_k, C_{k+1}, D_{k+1} account for the state, input, output, and feed-through matrixes, respectively.

In practice, it is not possible to evaluate the response of all degrees of freedom of a structure, specifically the rotational one, due to the complexity and high cost. Besides, the measured responses contain uncertainties due to the measurement noises. Thus, to determine the system matrices at every interval, using the system input measurement and responses of some structural degrees of freedom, even for linear systems, pose serious difficulties. The system state can be established using the Kalman filter (KF), as proposed by Kalman [63] in 1960. The KF algorithm is a forecasting and adjustment method to estimate the mean and the covariance of a linear system's state vector by minimizing the estimated state's variance. This KF algorithm predicts the following step values of a priori estimates of the state and the covariance of the estimation error ($\widehat{x}^-_{k+1}$, $P^-_{x,k+1}$). To improve the anticipated values of the system state and its covariance matrix, the variation between the estimated and evaluated responses of the system ($y_{k+1} - \widehat{y}^-_{k+1}$) can be assessed by employing an a priori state estimate. Notably, this prediction-updating process has been repeated for the next step. The details of the KF algorithm are presented in Fig. 1. A more detailed discussion can be found in the work of Simon [36].

2.1. Extended Kalman filter (EKF)

Eqs. (1) and (2) can be employed to discretely evaluate a nonlinear system's governing equations. For nonlinear systems, the state of the system or the input or both at the subsequent step of the time is not directly involved in the system and measurement equations at the current time step and next time step. The time-evolution of the probability distribution of nonlinear system states can be represented by many approaches. One of these methods is the conditioned Fokker-Planck differential equation [64], for which finding an explicit solution is often challenging. Thus, the KF algorithm may not be employed for the prediction-correction of these systems. Several strategies have been proposed to employ the KF algorithm for these systems, including the extended Kalman filter (EKF) method. We can apply the first-order Taylor series expansion about the operative point to linearize a nonlinear state-space system around the latest estimated state. Afterward, the KF prediction-updating method is employed to obtain the evaluation for predicting the subsequent time-step linearization of a linearized system. The Taylor series expansion of Eq. (1) around the $\widehat{x}^+_k$ operative point (a posteriori estimate) can be expressed as follows:

$$\begin{aligned} x_{k+1} = & \left[f_k(\widehat{x}^+_k, u_k) + \left.\frac{\partial f_k(x, u_k)}{\partial x^T}\right|_{x=\,\widehat{x}^+_k} (x_k - \widehat{x}^+_k) + H.O.T \right] + w_k \rightarrow x_{k+1} \\ & \cong A_k x_k + \widetilde{u}_k + w_k \end{aligned} \tag{5}$$

where $\widetilde{u}_k = f_k(\widehat{x}^+_k, u_k) - A_k \widehat{x}^+_k$ and $A_k = \left.\frac{\partial f_k}{\partial x^T}\right|_{x=\,\widehat{x}^+_k}$.

The subsequent value of the state vector and the covariance of the system state can be determined using Eqs. (6) and (7):

$$\widehat{x}^-_k = f_k(\widehat{x}^+_{k+1}, u_k) \tag{6}$$

$$P^-_{x,k+1} = A_k P^+_{x,k} A^T_k + Q_k \tag{7}$$

To assess the subsequent evaluation of the system state vector and the covariance system state, the evaluation equation should be linearly dispersed around a priori state estimate point as follows:

$$\begin{aligned} y_{k+1} = & \left[g_{k+1}(\widehat{x}^-_{k+1}, u_{k+1}) + \left.\frac{\partial g_{k+1}(x, u_{k+1})}{\partial x^T}\right|_{x=\,\widehat{x}^-_{k+1}} (x_{k+1} - \widehat{x}^-_{k+1}) + H.O.T \right] \\ & + \eta_{k+1} \rightarrow y_{k+1} \cong C_{k+1} x_{k+1} + \widetilde{z}_{k+1} + \eta_{k+1} \end{aligned} \tag{8}$$

where $C_{k+1} = \left.\frac{\partial g_{k+1}}{\partial x^T}\right|_{x=\,\widehat{x}^-_{k+1}}$ and $\widetilde{z}_{k+1} = g_{k+1}(\widehat{x}^-_{k+1}, u_{k+1}) - C_{k+1}\widehat{x}^-_{k+1}$.

Therefore, the following results can be achieved:

$$\widehat{y}^-_{k+1} = g_{k+1}(\widehat{x}^-_{k+1}, u_{k+1}) \tag{9}$$

$$P^-_{xy,k+1} \cong P^-_{x,k+1} C^T_{k+1} \tag{10}$$

$$P^-_{y,k+1} \cong C_{k+1} P^-_{x,k+1} C^T_{k+1} + R_{k+1} \tag{11}$$

The prediction-updating procedure of a nonlinear system can be derived using Eqs. (6), (7), and (9)-(11). In the above relations, the state equation around $\widehat{x}^+_k$ and the measurement equation around $\widehat{x}^-_{k+1}$ were

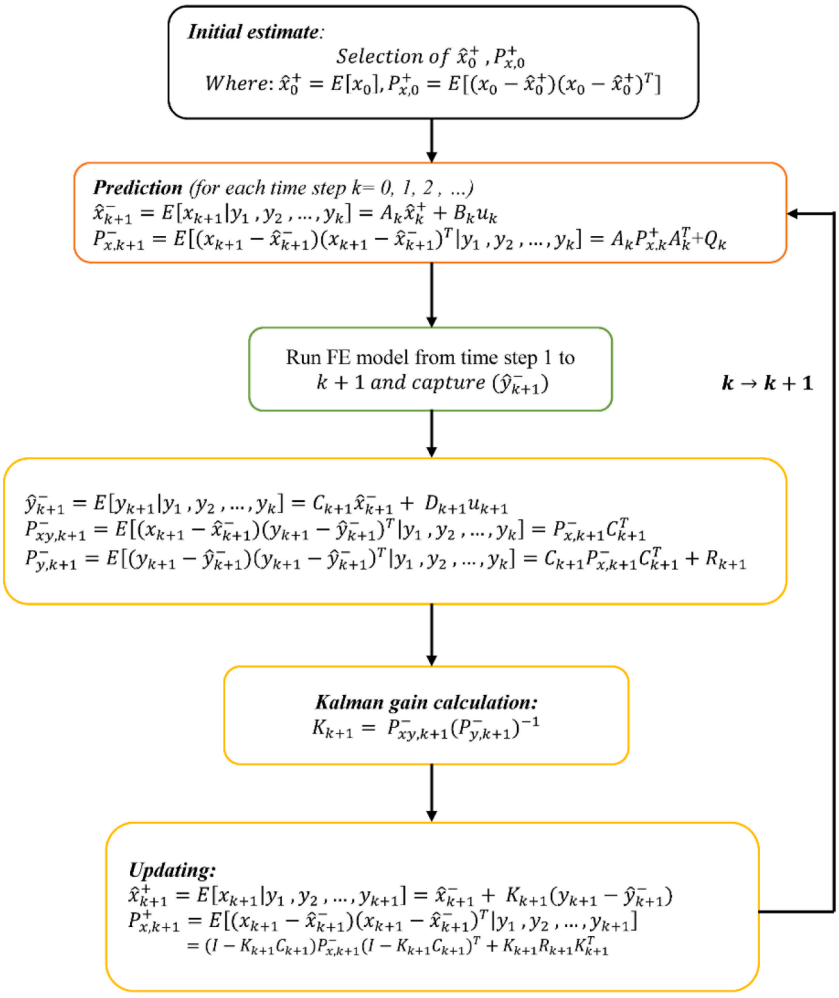

Fig. 1. Schematic representation of discrete-time KF algorithm.

linearized. This process can be explained as follows: In the state equation, since we are in the time update phase, the best answer is the a posteriori estimate from the previous step. To linearize the measurement equation, since we are in the measurement update phase and intend to update the measurement, the best estimate is the a priori state of the current step.

As shown in Eq. (8), the EKF method demands calculating the structural FE response sensitivities for unknown parameters. Two well-known differentiation techniques, namely the finite difference method (FDM) [65] and the direct differentiation method (DDM) [66], are employed for computing these coefficients. In this study, FDM is used to calculate the sensitivity coefficients because it provides fewer convergence issues in practical applications and lower computational costs.

It should be emphasized that using first-order linearization results in some errors in system identification. Therefore, it may cause large errors around the wrong results for highly nonlinear systems. Several approaches have been suggested to consider the inaccuracies resulting from the elemental first-order approximation intrinsic to the EKF implementation. Among these methods, the iterative Kalman filter (IKF) [67,68] or second or higher filter orders [69–71] contain achievable and well-matched estimation error reduction in specific application areas. The unscented Kalman filter (UKF) has stemmed from the research work of Julier and Uhlman, who presented the idea of the unscented transforms and developed it for the problem of recursive analysis and estimation. The following summarizes the UKF.

2.2. Unscented Kalman filter

The UKF was established based on a less complicated concept to approximate a probability distribution than an arbitrary nonlinear transformation. Consequently, the probability density function (PDF) of the system state at t_k, $P(x_k|y_{1:k})$, where $y_{1:k} = [y_1^T, y_2^T, \dots, y_k^T]^T$, can be estimated using a Gaussian distribution. Thus, the posterior PDF of the system state at the next step $P(x_{k+1}|y_{1:k})$, can be evaluated using a Gaussian vector with the following mean and covariance vectors:

$$\hat{x}_{k+1|k+1} = \hat{x}_{k+1|k} + K_{k+1}\left(y_{k+1} - \hat{y}_{k+1|k}\right) \tag{12}$$

$$P_{k+1|k+1} = P_{x,k+1|k} - K_{k+1}P_{y,k+1|k}K_{k+1}^T \tag{13}$$

where the $\hat{x}_{k+1|k+1}$ and $P_{k+1|k+1}$ denote estimates of the mean and covariance matrix of x_{k+1} given $y_{1:k+1}$, and $\hat{y}_{k+1|k}$ is the evaluation of the mean of y_{k+1} given $y_{1:k}$, and the Kalman gain matrix (K_{k+1}) is defined as:

$$K_{k+1} = P_{xy,k+1|k}\left(P_{y,k+1|k}\right)^{-1} \tag{14}$$

Solving a series of multiple integrals, rarely having closed-form solutions, results in defining the covariance matrices $P_{x,k+1|k}$, $P_{y,k+1|k}$, and $P_{xy,k+1|k}$. Therefore, numerical integration should be used to solve these multiple integrals. In this case, the unscented transformation (UT) method [72] is considered. In this approach, a group of deterministically chosen collection points, called sigma points (SPs), is employed to illustrate a randomly distributed vector Z. Hence, the mean and

covariance matrices of the sample derived from the SPs accurately correspond to the real mean and covariance matrices of the vector Z, which is randomly distributed. The SPs propagated through the nonlinear function can be used to capture the exact mean and covariance matrix of a nonlinear function up to the second-order of its Taylor series expansion.

The UT in this study is not the superior one implemented to solve various engineering problems. Different feasible UTs can be implemented if computational savings is the first priority, e.g., Simplex UT [73], Spherical UT [39], and Scaled Spherical Simplex UT [74] with decreased sigma points. Certainly, the nature of the noise must be known in most of these transformations. The difficulty with the simplex versions is the ratio between the weighting factors of different SPs can yield numerical problems. This issue, along with the instabilities induced by the use of experimental data, causes convergence problems. Therefore, equal weighting coefficients SPs case is used in this study.

2.3. Parameter estimation using EKF and UKF

FEMU assumes that the structure's model is discretized in the space state employing fiber-section force-based beam-column elements. Here, the nonlinearity can be considered member's integration points (IP). The member section is discretized using fibers. Constant parameters can describe the nonlinear uniaxial material constitutive model assigned to fibers, specifying their force-deformation.

Various accelerometers mounted on different points in a building structure record the structural responses and the input excitation during an earthquake. Moreover, several structural characteristics, including the sections, damping ratio, constraints, and constant parameters of behavioral models assigned to different fibers, can be specified to anticipate the structural response using the FE models. In this study, several complexities of the real structure have been disregarded, and constant parameters of material constitutive models assigned to different fibers and boundary constraints (the stiffness of beam-to-column connections and column-to-base) were considered in the modeling as the sources of uncertainties. Therefore, the main objective of this research is to determine the unknown parameters by minimizing the difference between the response of the real structure and that of the FE model. The following explains the methodology for estimating the mean and covariance of unknown parameters using measured data.

The nonlinear structural responses using the constant parameters (vectors of θ) can be established as follows:

$$y_{k+1} = g_{k+1}(\theta, u_{k+1}) + v_{k+1} \tag{15}$$

where $h(.,.)$ is the nonlinear vector-valued function, which indirectly parameterizes the model. The unknown parameters vector of θ can be defined as a random vector the evolution of which is described by a Gaussian Markov process [75]. Consequently, the system state equation, demonstrating the governing equations of the changes of unknown parameters and the measurement equation based on system output, is expressed as follows:

$$\theta_{k+1} = \theta_k + \gamma_k \tag{16}$$

$$y_{k+1} = g_{k+1}(\theta_{k+1}, u_{k+1}) + v_{k+1} \tag{17}$$

where γ_k is a zero-mean Gaussian white-noise process. Relying on this type of distribution for the discrepancy model can lead to approximate and biased identification outcomes [76]. Still, for numerical stability causes and employing EKF recursively, this assumption holds in this study. Intersently, Eqs. (16) and (17) are identical to (1) and (2), except that the process equation is expressed linearly, while the measurement equation can be considered a nonlinear equation. For this reason, solving the nonlinear equation and estimating its parameters can be considered a significant challenge when using the EKF and UKF methods.

2.4. Parameter estimation framework

In the event of seismic excitation, the governing equation of a nonlinear finite element model, which has been discretized at time- step $k + 1$, can be described as follows:

$$M(\theta)\ddot{q}_{k+1}(\theta) + C(\theta)\dot{q}_{k+1}(\theta) + r_{k+1}(q_{k+1}(\theta), \theta) = -MI\ddot{u}_{g,k+1} \tag{18}$$

where I and $\ddot{u}_g$ denote the influence vector and the input ground acceleration, respectively. Also, q, $\dot{q}$, and $\ddot{q}$ are the structural model displacements, velocity, and acceleration, respectively. M and C are the mass and damping matrices. $r(.,.)$ is the internal restoring force vector, which is directly dependent on unknown parameters and indirectly on unknown parameters through $q(\theta)$. The absolute acceleration of the structure can be obtained via the following relations:

$$y_{k+1} = L_y\left(\ddot{q}_{k+1} + I\ddot{u}_{g,k+1}\right) + v_{k+1} \tag{19}$$

Combining Eqs. (18) and (19) gives the absolute acceleration of the structure as:

$$y_{k+1} = g_{k+1}\left(\theta, \left[\ddot{u}_{g,k+1}\right], \dot{q}_0, q_0\right) + v_{k+1} \tag{20}$$

where y_{k+1} accounts for the absolute acceleration value, $[\ddot{u}_{g,k+1}] = [\ddot{u}_{g,1}, \ddot{u}_{g,2}, \ldots, \ddot{u}_{g,k+1}]^T$ is the input ground acceleration from time step 1 to time step $k + 1$, and q_0 and $\dot{q}_0$ denote the initial displacement and velocity of the structure, respectively, wherein the values can be equal to 0 at the initial condition for the sake of simplicity.

Considering the random distribution of θ characterized by a Gaussian Markov Process, the estimation of the unknown parameters can be expressed as:

$$\theta_{k+1} = \theta_k + \gamma_k \tag{21}$$

$$y_{k+1} = g_{k+1}\left(\theta_{k+1}, \left[\ddot{u}_{g,k+1}\right]\right) + v_{k+1} \tag{22}$$

where $\gamma_k \sim N(0, Q_k)$.

The second-order statistics of the process noise γ are considered constant in each analysis, i.e., $Q_k = Q$. The process noise covariance matrix is characterized as $Q_k = E(\gamma\gamma^T)$. This matrix is designated diagonally, whose elements on the diagonal are the process noise variances related to the parameters to be evaluated. In this study, these variances are characterized as $q^2 \times Diag([\theta_i^2])$, where q is the root mean square error (RMSE) of each component of the process noise. This parameter is taken as a percentage of the initial assessment of the related material parameter. Different values are considered for this parameter. Enhancing the process noise variance increases the estimation uncertainty and the relevant significance assigned by the Kalman filter to the response measurements versus the latest prior estimation of the parameters. Briefly, the size of the process noise variance exploits the step size of the evolution of the parameter vector estimations [36].

According to the equations mentioned in the previous sections, the EKF and UKF methods can be employed recursively to estimate the unknown parameters. Fig. 2 and Fig. 3 demonstrate the process of these algorithms, respectively.

3. The sensor placement methodology

The precise prediction of a structural system behavior based on measured response is crucial because it can promote structural health monitoring and reliability analysis. Therefore, due to the limited number of measurements, and small size of samples from one side, and numerous uncertainty sources from another side, it is necessary to develop methodologies that show the best location and type of measured data. Among the many proposed techniques, information entropy (IE)

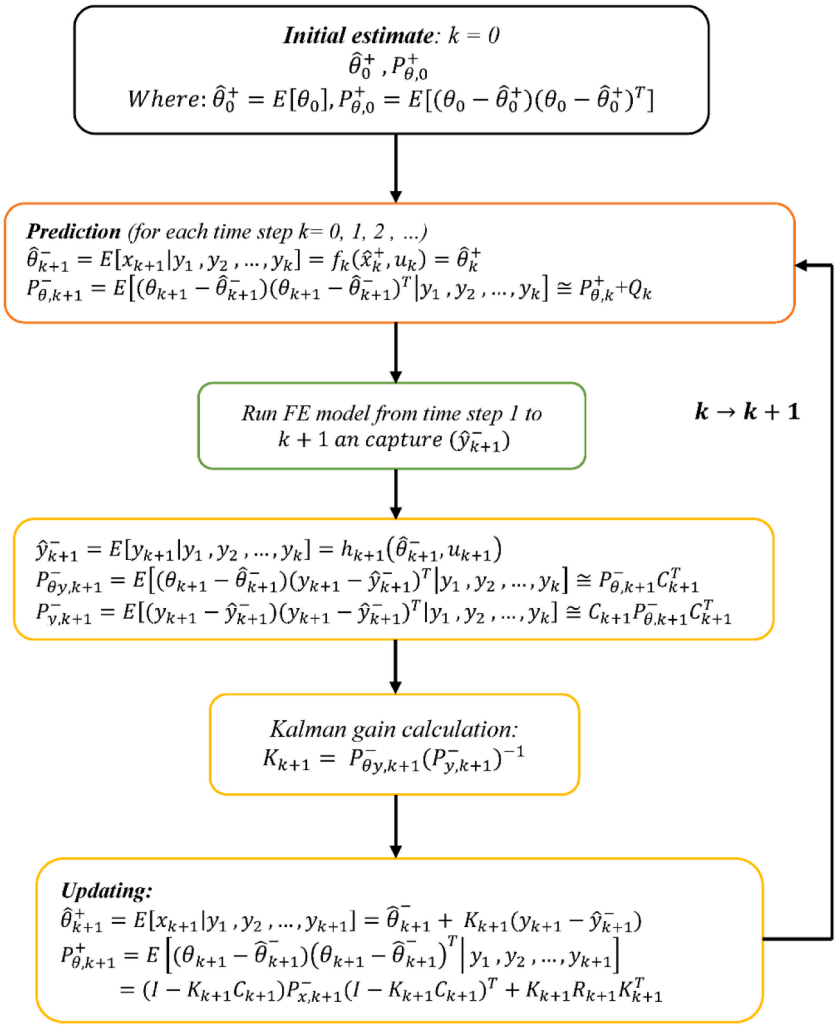

Fig. 2. Schematic illustration and flowchart of discrete-time EKF for parameter estimation under base excitation.

[77] and cross-entropy(CE) [78] can be mentioned as the two fast and simple methods to determine the best combination and location of responses for system identification. In this study, IE is used regarding its rather straightforward usage.

Using the structural degrees of freedom (DOF) and the observed DOF with N_d and N_o, respectively, the acceleration response of a building structure at a *kth* time step, i.e., $t_k = k\Delta t$, is obtained as follows:

$$y_{k+1} = L_y[\ddot{q}(k,\theta) + v(k,\theta)] \tag{23}$$

where $L_y \epsilon R^{N_o \times N_d}$ accounts for the output matrix with only one non-zero element, which is equal to unity in each row. The observed DOFs and N_o can be expressed using a sensor configuration vector as follows:

$$\delta = L_y^T \widehat{U}_n \tag{24}$$

where $\widehat{U}_n \epsilon R^{N_o}$ denotes a vector whose entire elements can be equal to unity. Also, for $\delta \epsilon R^{N_d}$, in the case of observing the DOF *i*, the *ith* element can be equal to unity, and it is 0 in the rest of the cases.

As stated previously, the optimal value of θ can be obtained by minimizing the real structural response regarding the anticipated one from the finite element model, as follows:

$$G(\theta) = \frac{1}{N_t N_o} \sum_{k=1}^{N_t} \| y_k - L_y \ddot{q}_k(\theta) \|^2 \tag{25}$$

where $\| \cdot \|$ denotes the square norm, and N_t is the number of estimated time steps. A PDF using probability models can be employed to evaluate the uncertainties associated with the parameter θ. To achieve the posterior PDF of parameter θ, which is dependent on a specified configuration of a sensor and a group of valued data, an asymptotic approximation can be used as follows [79]:

$$P(\theta|\delta, D) = CG(\theta)^{-\frac{N_t N_o}{2}} \pi(\theta) \tag{26}$$

where C denotes a normalized constant, D shows the measured data, and $\pi(\theta)$ indicates the prior distribution of the parameter θ.

With reference to a non-informative prior distribution $\pi(\theta)$ and a wide range of noted data points, N_t, the posterior PDF particularly reaches its peak at D, where $\widehat{\theta}$ is the optimal parameter θ.

3.1. Information entropy

The optimal value of $\widehat{\theta}$ and the behavioral parameters of a structure with the highest likelihood following D are considered known. It is noted that for a specified configuration of sensors δ, the information entropy, which tacitly relies on the recorded data D, $\widehat{\theta}$, and $\widehat{\sigma}^2 = G(\widehat{\theta}, D)$, can be defined as [80]:

$$H(\widehat{\theta}, \delta) = E_\theta[-\ln P(\theta|\widehat{\theta}, \delta)] \tag{27}$$

where E_θ is the mathematical expectation in terms of θ. Employing Eq. (26), the information entropy can be obtained by [77]:

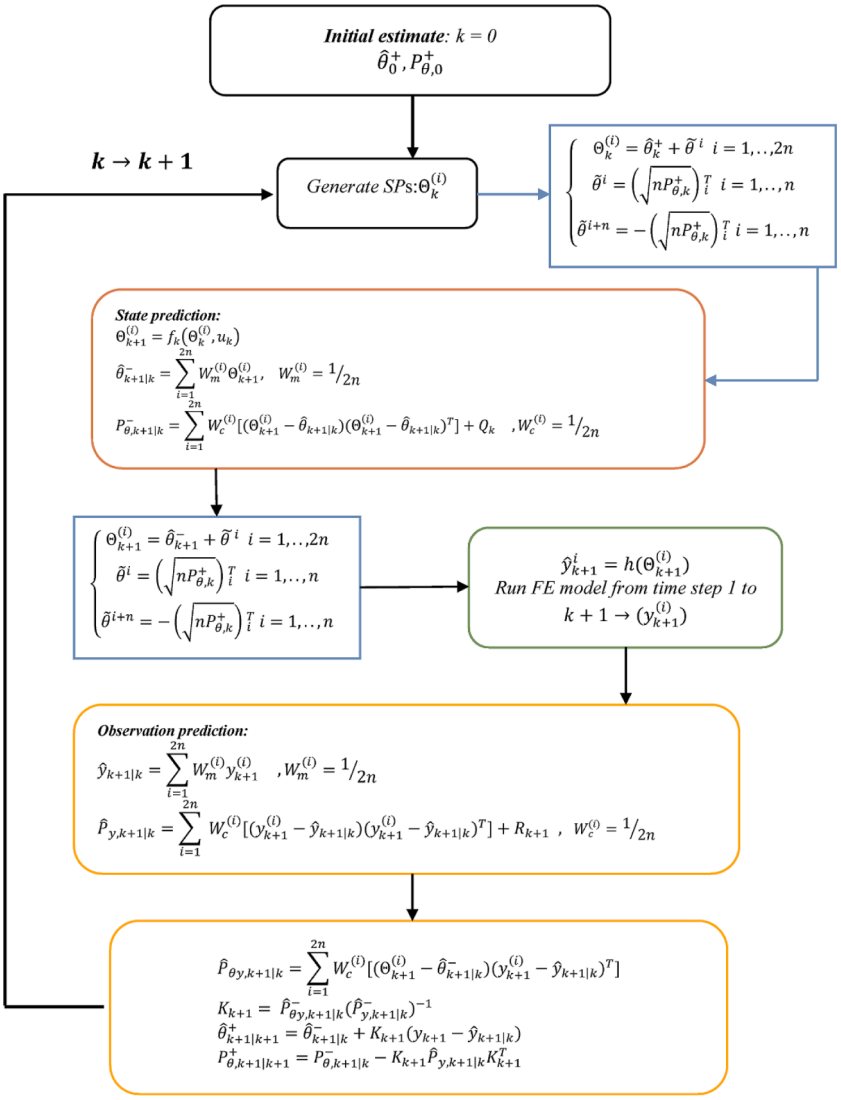

Fig. 3. Schematic illustration of discrete-time UKF for parameter estimation under base excitation.

$$H(\widehat{\theta},\delta) = \frac{1}{2}N_\theta\left[\ln(2\pi) + 1 + \ln\widehat{\sigma}^2\right] - \frac{1}{2}\ln\det Q(\delta,\widehat{\theta}) \tag{28}$$

where N_θ stands for the number of uncertain model parameters. The elements of the matrix $Q(\delta,\widehat{\theta})$ can be evaluated by [81]:

$$Q_{ij}(\delta,\widehat{\theta}) \approx \sum_{k=1}^{N_t}\left[\frac{\partial q(k,\theta)}{\partial\theta_i}^T L_y^T L_y \frac{\partial q(k,\theta)}{\partial\theta_j}\right] \tag{29}$$

For the sake of simplicity, the elements of matrix $Q(\delta,\widehat{\theta})$ can be given by:

$$Q_{ij}(\delta,\widehat{\theta}) = \sum_{i=1}^{N_d}\delta_i P(\widehat{\theta}) \tag{30}$$

where the elements of the matrix $P(\widehat{\theta})$ can be represented as:

Consequently, determining the optimal placement of sensors can be considered to minimize the information entropy expressed based on Eq. (28). According to Eq. (28), $\det Q(\delta,\widehat{\theta})$ should be maximized to minimize the $H(\widehat{\theta},\delta)$. Also, all possible modes of sensor placement should be considered to find the maximum value of the parameter $\det Q(\delta,\widehat{\theta})$ with respect to a base mode. To obtain the optimum base mode configuration, it can be assumed that all sensors have been installed in all structural DOFs, and the structural responses can be employed for measuring the information entropy. Accordingly, considering the value of the information entropy ($H(\widehat{\theta},\delta) = H_0$), the information entropy difference for a given configuration of sensors with respect to the base mode can be computed as:

$$H - H_0 = 0.5 \times \ln\frac{|Q(\delta_0,\widehat{\theta})|}{|Q(\delta,\widehat{\theta})|} \tag{32}$$

where $|.|$ denotes the determinant. It is presumed that s^2 is the geometric value of the mean of the principal variances of the covariance matrix $\sigma_0^2 Q(\delta,\widehat{\theta})^{-1}$ of the dispersion $P(\theta|\widehat{\theta},\delta)$. To obtain the value of s^2, the general spreading of the distribution $P(\theta|\widehat{\theta},\delta)$ around the mean value of the model parameters of the structure can be used. The parameter-uncertainty ratio (PR) can be derived by assuming two different distributions following the vector of sensor configuration [77]:

$$\frac{S}{S_0} = \exp\left(\frac{H - H_0}{N_\theta}\right) \tag{33}$$

Consequently, the ratio of arithmetical means of the standard deviations merely relies on the variations of information entropy and various parameters of the model. Hence, the ratio is alternatively employed for measuring the variations between the two cases in terms of

uncertainty. More particularly, increasing or decreasing the entropy relies on increasing or decreasing the parameter-uncertainty ratio. However, the *PR* can be equal to unity in the case of the two sensor configurations with identical information entropy.

In the case of implementation, due to the explicit comparability of the dispersion of the PDF of θ around its mean values using the parameter-uncertainty ratio, the variations of the uncertainty between cases can be expressed with respect to the *PR* rather than the entropy ratio.

4. Test structure

The 1:8 scale prototype structure used in this study is shown in Fig. 4. This structure is made of elastic elements linked with plastic hinge components. A mass simulator is connected to the test structure to implement the effects caused by seismic masses, gravity loads, and *P – Delta* phenomenon. Furthermore, this study takes advantage of a bracing frame to constrain the out-of-plane motion of the experimental system. To adequately simulate the deterioration modes, the plastic hinge elements were constructed with detailed components from A992 steel with a yield stress of 50 ksi located at both ends of the members. As shown in Table 1, a sequence of excitations, including white noise, sine-sweep, pulse-type excitations, and earthquake records, are considered for the test frame [82].

The structure was damaged under 100% load of the Canoga Park (CP) record of the 1994 Northridge earthquake (see Fig. 5), presenting the design-level earthquake (DLE) [82]. The test frame behaved elastically under 20% and 40% of the mentioned earthquake, while inelastic damage is observed under the DLE earthquake (Fig. 6). Determining the damage level of the test frame under different base excitations qualitatively, in addition to monitoring the amount of peak story drift ratios, was accomplished by investigating the residual displacement of the frame. Notably, the response of 20% of the Canoga Park record, white-noise excitation, and impulsive excitation are employed in calculating the IEM. According to the test results, only the bottom part of the first story column behaves nonlinearly. The beams of the first two stories demonstrate the maximum amount of nonlinearity. Meanwhile, a slighter level of nonlinearity is observed in the beams of the upper stories (Fig. 6). The deformation of all potential nonlinear regions of the frame was estimated using more than 247 data channels in the test frame. A data acquisition system with a sampling rate of 128 Hz was implemented to record all responses of the test system. The nonlinear region's time history response, including strain, deformation, and stress during different excitations, was recorded through strain gages and clip gages. Displacement transducers and accelerometers installed on the shake table, floors, and the mass simulator were operated to measure the displacement and acceleration responses in all directions. A comprehensive report of the test procedures is provided by Lignos et al. [82].

Fig. 4. Test structure, mass simulator, and bracing system on the SUNY-NEES shake table [82].

Table 1
Base excitation sequences for the scaled test structure.

Base excitation sequence	Base excitation	Scale	Description	Abbreviation
1	Canoga Park earthquake	20%	–	–
2	Canoga Park earthquake	40%	Service level earthquake	SLE
3	Canoga Park earthquake	100%	Design level earthquake	DLE
4	Llolleo earthquake	150%	Maximum considerable earthquake	MCE
5	Canoga Park earthquake	220%	Collapse level earthquake	CLE
6	Canoga Park earthquake	220%	Final collapse level earthquake	CLEF

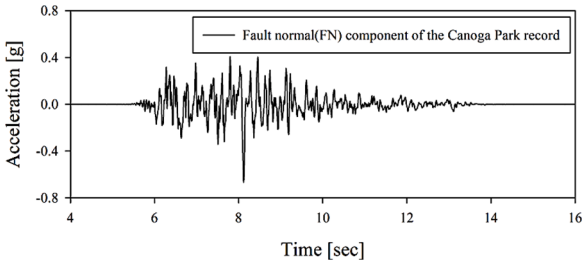

Fig. 5. Time history of the Canoga Park ground motion.

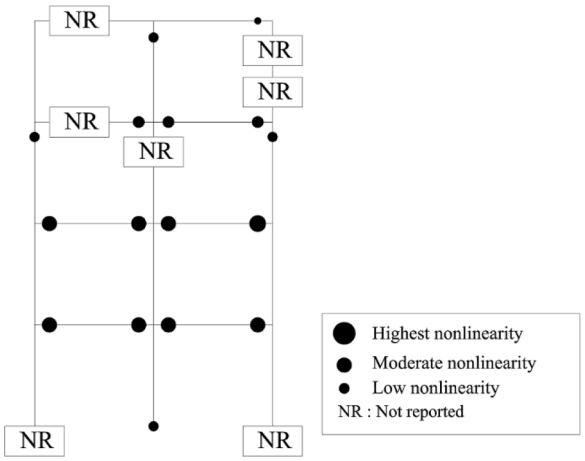

Fig. 6. The severities and locations of nonlinearity of the test structure under DLE.

5. Uncertainty development and FE models

The uncertainty of the FE model generates inaccurate estimations of the system response and its reliability. Therefore, it is significant to develop and evolve numerical models that consider the uncertain character of real structural systems. In this study, four models of the test frame with completely different aspects are evolved to consider the influence of various uncertainties. The FE modeling of the frame was performed using the OpenSees software [83]. The elements of the structure were modeled using the elements of the OpenSees, including the "linear elastic beam-column" and "nonlinear beam-column" with distributed plasticity. Hence, employing the distributed plasticity rather than the concentrated one can be considered among the uncertainties applied in the modeling. Using the distributed plasticity rather than the concentrated one leads to the material nonlinearity distribution along

several sections of the elements, referred to as the integration points (IPs). The sections are additionally discretized into fibers [84]. The uniaxial force-displacement response is assigned to each fiber according to the selected material model. Fig. 7 shows the stages of the structural component divisions of FE models. In the first model, which is the beam-column model with the distributed plasticity considering the G-M-P and BWBN hysteretic models, it is presumed that the structure behaves elastically except for the columns of the first story and the beams of the first two stories. The second model is identical to the first model except for semi-rigid connections at the bottom of its first-story columns. In contrast, for the third model, semi-rigid connections can be assumed for total beam-column connections.

Fig. 7(a) shows that the fourth model behaves as a shear frame with rigid beams. It is also assumed that the columns are merely allowed to rotate due to the slab diaphragm. Based on this Fig., 6 and 8 IPs of the Gauss-Lobatto quadrature for columns and beams, respectively, can be implemented for the numerical integration along the element length. Four fibers and one fiber have been used along the length and width of the web of the first story columns, respectively (Fig. 7b)). Six fibers and one fiber were assigned along the height and width of the webs of the beams of the first two stories, respectively. At the same time, one fiber is employed for the flange of columns and beams along their thickness.

To consider the uncertainties related to the material behavior model, we used two models in the fiber sections of all models: BWBN and G-M-P. Notably, regarding their simplicity of implementation in the state-space models, these models have been used for structural system identification with recursive algorithms. Unlike the G-M-P model, the parameters of the empirical BWBN model contained no tangible signification. The parameters of the BWBN model are extracted by developing a case-by-case study. In addition to the dependency of the parameters of this model on each other, multiplying its parameters resulted in problems, and different combinations of these parameters resulted in nearly identical responses. Unlike the BWBN model, the G-M-P model was advantageously calibrated. A brief description of each material behavior model and the way to select their parameters are stated in the following sections.

5.1. Hysteretic material model

5.1.1. G-M-P

The G-M-P material model is shown in Fig. 7(c). As can be seen, about 10 parameters were used to formulate this model. Among these parameters, E is the modulus of elasticity, F_y shows initial yield stress, and b is strain hardening ratio.To control the hysteretic behavior, Baushinger effects, and isotropic hardening, seven remaining empirical parameters were employed.

5.1.2. Bouc-Wen-Baber-Noori

In the BWBN material model shown in Fig. 7(d), stiffness and strength deterioration with no pinching were considered. In this model, the nonlinear restoring force of the system is given as:

$$R(x,z) = \alpha K_0 x + (1-\alpha)K_0 z \tag{34}$$

$$\dot{z} = \frac{A\dot{x} - \nu\beta|\dot{x}|\,|z|^{n-1}z - \nu\gamma\dot{x}|z|^n}{\eta} \tag{35}$$

$$A = A_0 - \delta_A \varepsilon \tag{36}$$

$$\nu = 1 + \delta_\nu \varepsilon \tag{37}$$

$$\eta = 1 + \delta_\eta \varepsilon \tag{38}$$

$$\varepsilon = \int_0^t \dot{z}\dot{x}dt \tag{39}$$

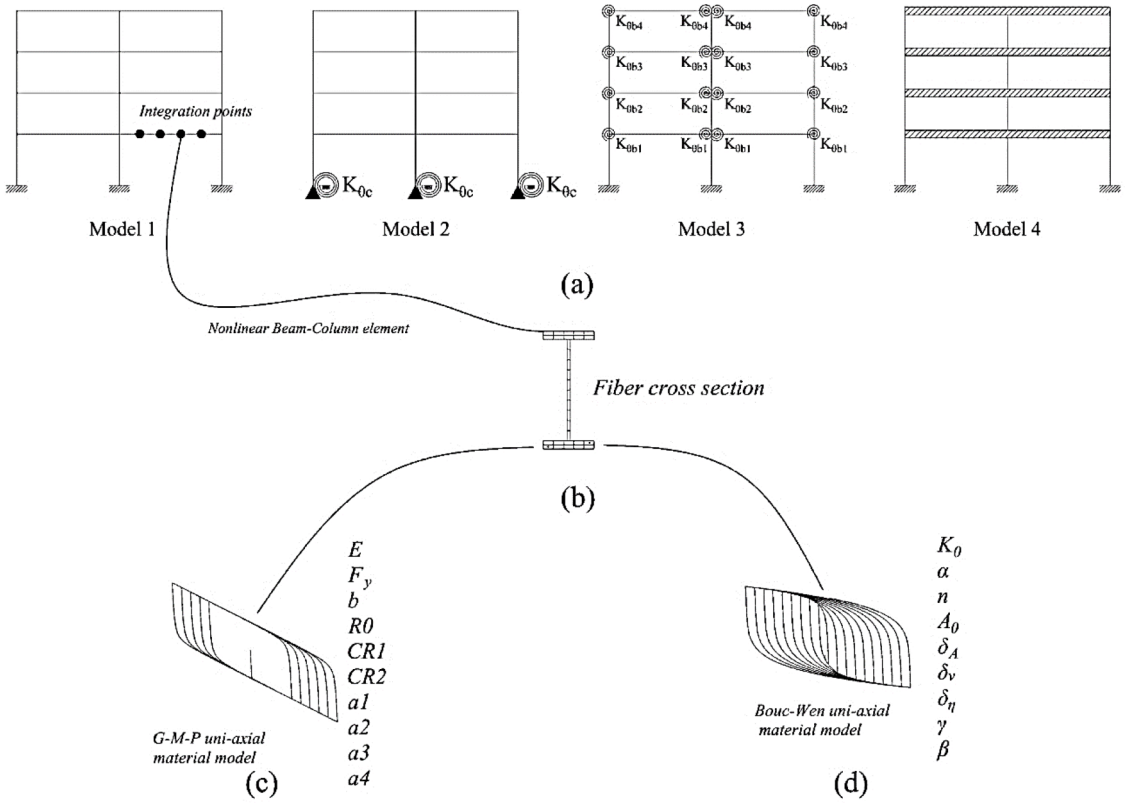

Fig. 7. Hierarchical discretization orders of nonlinear structural FE models, (a) different modeling asumption, (b) fiber cross-section for distributed beam-column elements, (c) G-M-P material model constitutive law and related parameters, and (d) BWBN material model constitutive law and related parameters.

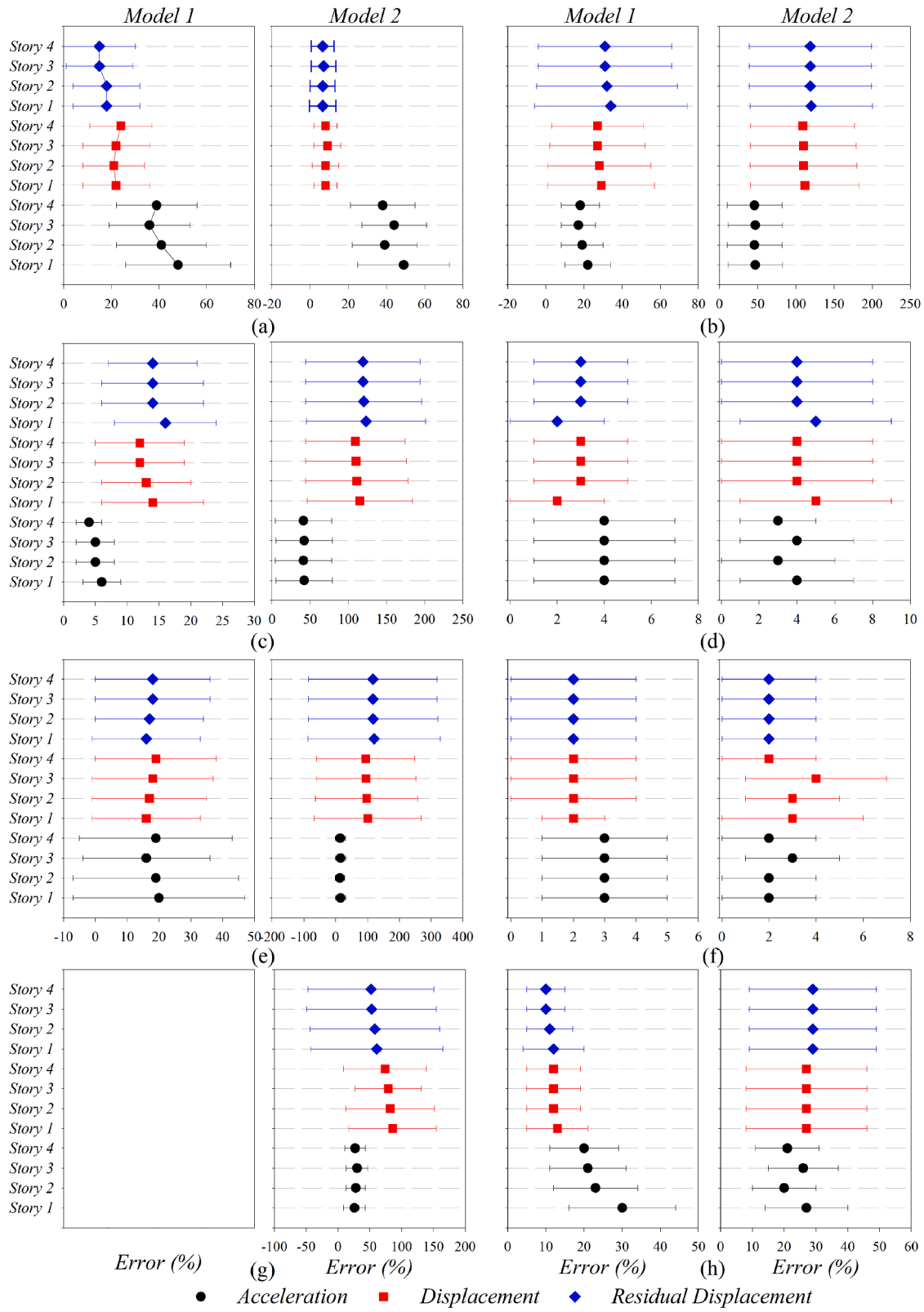

Fig. 8. The statistical properties for various sensitivity indicators of G-M-P hysteretic behavior for models 1 and 2: (a) $\boldsymbol{E}$, (b) $\boldsymbol{F_y}$, (c) $\boldsymbol{b}$, (d) $\boldsymbol{R}0$, (e) $\boldsymbol{CR}1$, (f) $\boldsymbol{CR}2$, (g) $\boldsymbol{K_\theta}$, and (h) $\boldsymbol{\xi}$.

where K_0 and z, respectively, stand for the initial tangent stiffness and the virtual nonlinear cyclic displacement of the structure; α, A, ν, β, γ, η, δ_A, δ_ν, δ_η and A_0 characterize the model; α is the post-yield stiffness ratio; ε is the hysteresis energy; A, β, and γ control the level of nonlinearity, where γ and β are identical values. In addition, n accounts for the sharpness of transition in the yield point, and η and ν control the deterioration of the model.

Employing all parameters of both material behavior models

increases the likelihood of an error during the identification process. To avoid this issue, the parameters affecting the structure's response at the DLE should be selected, while other parameters with minor effects should be considered definite. Thus, the effective parameters may be determined using sensitivity analysis (SA) and appropriate index selection.

SA and uncertainty analysis, with the latter more focusing on uncertainty quantification and uncertainty propagation, are usually performed jointly in many practical cases. There are many techniques for performing SA. Many of these techniques are designed to handle one or more of the restrictions of any particular problem, e.g., [85–88]. In one of the most straightforward methods of SA, the desired sensitivity criteria are calculated using the outputs of the resulting model. Consequently, a baseline model was selected, and the discrepancy between the responses of the simulated and baseline models can be used to specify the sensitivity of the model to varying its parameters. For this purpose, two general approaches were used: 1) the discrepancy between the residual displacement of several stories and 2) the variations of the acceleration responses of several stories of the simulated and baseline models. These general approaches can be determined by implementing the following equations:

$$e_{Res,i} = \frac{\left|Res_i^{Simulated} - Res_i^{Baseline}\right|}{\left|Res_i^{Baseline}\right|} \times 100 \tag{40}$$

$$e_{Acc,i} = \frac{\| Acc_i^{Simulated} - Acc_i^{Baseline} \|}{\| Acc_i^{Baseline} \|} \times 100 \tag{41}$$

where the superscripts *Simulated* and *Baseline* stand for the simulated and baseline model, respectively; *Res* and *Acc* denote the vectors of residual deformation and acceleration responses, respectively; and $\| . \|$ shows for the Euclidean norm value. To define 12 different indexes under DLE, the preceding equations were used in the following order: Indexes 1–4 demonstrate the acceleration responses of the first to fourth stories. Besides, indexes 5–8 indicate the displacement responses of the first to fourth stories, and indexes 9–12 report the residual displacement of the first to fourth stories. The exact values of the parameters of two material hysteretic models for the baseline mode are summarized in Table 2. For each analysis, the gravity forces were assigned in a quasi-static manner, followed by using the base excitation dynamically.

Newmark average acceleration method [89] was used to recursively incorporate the time-domain equation of motion using a frequency of 128 Hz through the nonlinear time-history analysis. Meanwhile, the Newton-Raphson method [89] was employed to iteratively figure out the incremental dynamic equilibrium equation nonlinearly at every individual time step. Tangent stiffness-proportional damping [89] can be used to idealize the properties of the damping energy dissipation over and above the material hysteretic energy of the frame. To this end, we assume varied damping ratios for the first mode. The mean (μ) and standard deviation (σ) for various sensitivity indicators of different models are illustrated in Fig. 8, Fig. 9, Fig. 10, Fig. 11. These figures show the mean and change of time-domain error metrics. For the time-domain metrics, the horizontal lines in the plot depict the error range in the four stories, and the black, red, and blue dots denote the mean values. By examining these figures, the following conclusions can be made:

- A good match existed between the acceleration and displacement criteria, suggesting that both criteria are suitable for determining the sensitive parameters.
- For model-1, the parameters of the G-M-P material model (i.e., E, F_y, b and $CR1$) affect the overall behavior of the frame. The most significant effect pertains to the E parameter, followed by F_y and $CR1$ parameters, and then the b parameters. A negligible impact of the unknown parameter $R0$ was noticed for the weak earthquake, which is comparable to that of the unknown parameter b. Several parameters were employed to assess the structural system concerning the BWBN behavioral model. The most significant effect relates to the parameter K_0 and α, while the parameter n has the lowest effect.
- The structure experiences a slight nonlinearity under the DLE, and the displacement criterion was considered merely for determining the dimensions of the structural elements of the moment-resisting frame structure and prevailed over the strength criteria. As a result, the parameters related to the stiffness of the structure (i.e., the E and K_0) have the greatest impact compared to other parameters.
- For model-2, similar to the parameter E, the effect of parameter K_θ for the G-M-P model, and the parameters K_0 and α for the BWBN material model are considerably higher than other parameters. This result indicates that the greater the number of parameters pertaining to the structure's stiffness, the lower the effect of parameters relating to the strength of the structure. This is the case for model-3, wherein the rigidity of the beam-column connections was considered an unknown parameter.

6. EKF and UKF frameworks results

6.1. State estimation results under DLE

Both EKF and UKF algorithms were performed using MATLAB software [90] interfaced using the OpenSees platform. Therefore, it is possible to determine the responses of the finite element models and the response sensitivity. To conduct the analysis, the initial values and the initial covariance matrix, implying the uncertainties related to the initial assumptions, were assumed for the parameters of each behavior model. To examine several uncertainties related to the considered data feature, four modes of structural responses for nonlinear model calibration through the EKF and UKF were implemented: 1) the acceleration responses of all stories(Case_1), 2) the acceleration responses of all stories along with the displacement responses of the first and third floors (Case_2), 3) the acceleration responses of all stories along with the displacement responses of the second and fourth floors(Case_3), and 4) the acceleration and displacement responses of all stories(Case_4). The analysis was conducted using several factors, including the element selection, the number of IPs along the length of the elements, the number of fibers, different types of methods for solving nonlinear equations, and the time-step of each time interval. These factors are identical to those of the sensitivity analysis section mentioned in the paper. Table 3 presents various scenarios for identifying the test frame.

In this study, 100 analyses were conducted to estimate the parame-

Table 2
The assigned values of parameters of two material hysteretic models for the baseline models.

G-M-P material model								
Parameters	$E(MPa)$	$F_y(MPa)$	b	$R0$	$CR1$	$CR2$	$K_\theta = N^* \times 6EI/l$	ξ
	2e5	350	0.02	15	0.6	0.15	10	0.02
BWBN material model								
Parameters	α	n	δ_ν	δ_η	δ_A	γ	$K_\theta = N^* \times 6EI/l$	ξ	A_0
	0.5	1.0	0.2	0.2	0.0	300	10	0.02	1.0

*The N is considered as a variable.

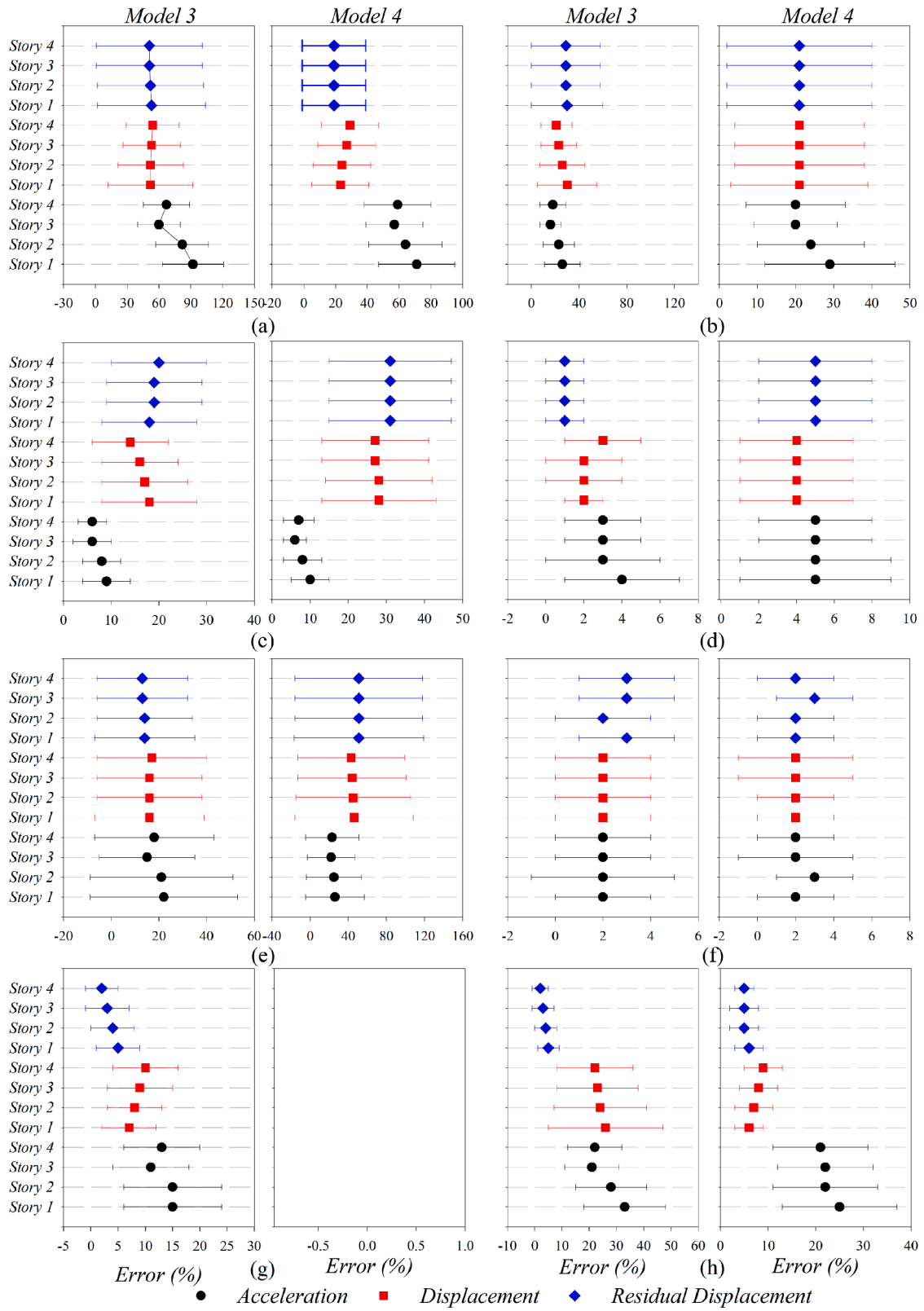

Fig. 9. The statistical properties for various sensitivity indicators of G-M-P hysteretic behavior for models 3 and 4: (a) $\boldsymbol{E}$, (b) $\boldsymbol{F_y}$, (c) $\boldsymbol{b}$, (d) $\boldsymbol{R0}$, (e) $\boldsymbol{CR1}$, (f) $\boldsymbol{CR2}$, (g) $\boldsymbol{K_\theta}$, and (h) $\boldsymbol{\xi}$.

ters of the behavior model. The analyses involve different initial values, the covariance of the estimation error, and the covariance matrix of process noise. Here, the lower the values of the elements of the covariance of the estimation error matrix, the lower the rate of convergence and vice versa; however, selecting the elements of the covariance matrix with higher values reduces the stability of the framework [36]. The initial values of the unknown parameters ($\hat{\theta}_0^+ = r_i \times \theta_{Assumed}$) and related estimated covariance matrix for both material behavior models are

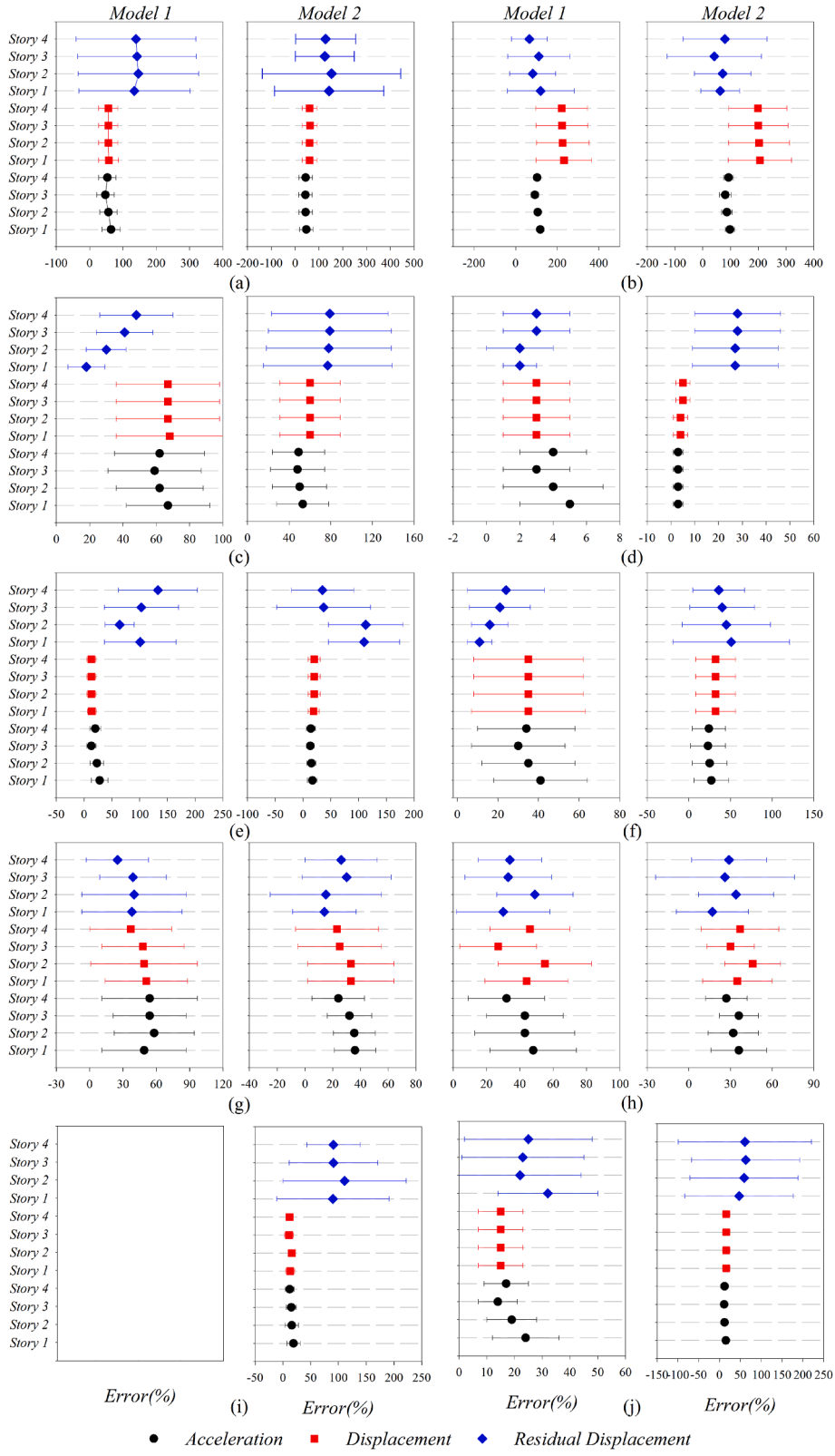

Fig. 10. The statistical properties for various sensitivity indicators of the BWBN hysteretic behavior for models 1 and 2: (a) $\boldsymbol{\alpha}$, (b) $\boldsymbol{K}_0$, (c) $\boldsymbol{n}$, (d) $\boldsymbol{\delta}_\nu$, (e) $\boldsymbol{\delta}_\eta$, (f) $\boldsymbol{\gamma}$, (g) $\boldsymbol{A}_0$, (h) $\boldsymbol{\delta}_A$, (i) $\boldsymbol{K}_\theta$, and (j) $\boldsymbol{\xi}$.

presented in Table 4 and Table 5. The use of r_i indicates that for each unknown parameter, a coefficient of the value mentioned in the table is supposed. In this study, $P^{+}_{\theta,0}$ is represented as a diagonal matrix, suggesting that initial estimates of the unknown parameters of the behavioral model are considered without relation. For instance, the diagonal elements of matrix $P^{+}_{\theta,0}$ for the model_4 and G-M-P material model are: $(pE_{true})^2$, $(pF_{y,true})^2$, $(pb_{true})^2$, $(pCR1_{true})^2$, and $(p\xi_{true})^2$. Here, p is the coefficient of variation of the initial parameter estimations.

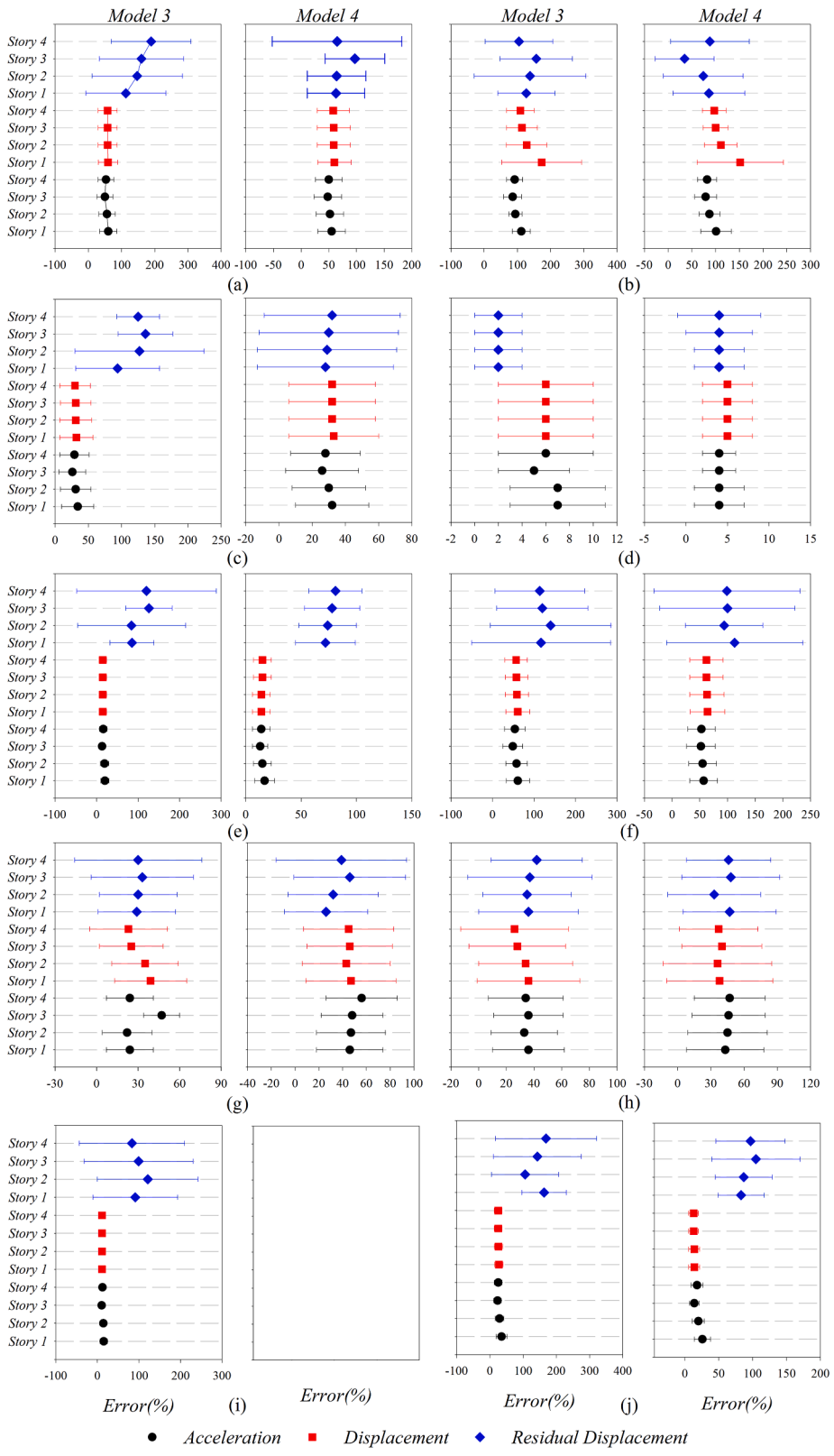

Fig. 11. The statistical properties for various sensitivity indicators of the BWBN hysteretic behavior for models 3 and 4: (a) $\boldsymbol{\alpha}$, (b) $\boldsymbol{K}_0$, (c) $\boldsymbol{n}$, (d) $\boldsymbol{\delta}_\nu$, (e) $\boldsymbol{\delta}_\eta$, (f) $\boldsymbol{\gamma}$, (g) $\boldsymbol{A}_0$, (h) $\boldsymbol{\delta}_A$, (i) $\boldsymbol{K}_\theta$, and (j) $\boldsymbol{\xi}$.

The algorithm has gradually marched forward in time, the number of structural responses increased, the effect of considering different initial values of parameters, and their covariance coefficients decreased. There is no correlation between the assumed initial and obtained values of parameters of behavioral materials.

The number of SPs in the UKF method is twice the number of system states, n (unknown parameters). Therefore, in each time step, we need to run the FE model of the test frame 2n times. In the EKF method, since

Table 3
Recursive algorithms, modeling assumptions, material model behavior, and type of data features in system identification.

Identification algorithm	Structural FE model type (Fig. 7)	Hysteretic material model (Fig. 7)	Data feature characteristics	No. of analysis
EKF(Fig. 2)	Model 1	G-M-P	Cases_1–4	100
		BWBN	Case_1: acceleration	100
	Model 2	G-M-P	responses of 1st to	100
		BWBN	4th stories	100
	Model 3	G-M-P	Case_2: acceleration	100
		BWBN	responses of 1st to	100
	Model 4	G-M-P	4th and	100
		BWBN	displacement	100
UKF(Fig. 3)	Model 1	G-M-P	responses of 1st and	100
		BWBN	3rd stories	100
	Model 2	G-M-P	Case_3: acceleration	100
		BWBN	responses of 1st to	100
	Model 3	G-M-P	4th and	100
		BWBN	displacement	100
	Model 4	G-M-P	responses of 2nd	100
		BWBN	and 4th stories	100
			Case_4: acceleration and displacement responses of 1st to 4th stories	

sensitivity must be calculated for each unknown parameter, the FE model must be run n times in each time step. Hence, the time required for UKF is approximately twice as long.

Fig. 12 and Fig. 13 present the variations of parameters of the G-M-P and the BWBN material models, respectively, normalized to their mean values for different models of Case_1. Also, the statistical values obtained for two material model parameters are shown in Table 6 and Table 7.

Based on the information presented in Fig. 12 and Fig. 13, it can be concluded that selecting different initial values of parameters and the covariance matrix with high dispersion does not lead to disparate final values of some parameters, especially the Young Modulus, E, of the G-M-P behavior model, and the k_0 and α of the BWBN behavioral model. These limited variations demonstrate the high accuracy of estimating the mentioned parameters. In other words, the values of these parameters relevant to the structure's stiffness were determined at the beginning of the analysis. In this stage, accelerations with low amplitudes apply to the structure, and the structure behaves elastically. Therefore, the linearization technique may not be used. Moreover, because of the correlation between the BWBN model's variables and their dependency on the parameter $\dot{z}$, the process of recognizing these parameters at the beginning of the seismic excitation accompanies unexpected difficulty. As a result, the Young Modulus derived from the G-M-P model was determined with more accuracy than the corresponding parameters of the BWBN model. In the third and fourth models, due to the modeling errors, some fluctuations were introduced for the BWBN model's variables, suggesting the low accuracy of the EKF and UKF methods in predicting the structural responses.

Fig. 14, 15, 16, Fig. 17. present the anticipated displacement responses of different stories, along with the responses of the experimentally tested structure for model_1 considering the G-M-P and the BWBN material model and different modes of structural responses through the EKF and UKF.

The accuracy of various models is quantified using several approaches, such as the differences between the tested structure and the calibrated one (during strong shaking), defined as follows:

$$e_i = \frac{\| r_i^{Calibrated} - r_i^{Test} \|}{\| r_i^{Test} \|} \tag{42}$$

where $r^{calibrated}$ and r^{Test} are the calibrated and tested responses, respectively. The error matrix of the displacement and acceleration responses of both behavior models through the EKF and UKF are demonstrated in Fig. 18 and Fig. 19. As can be seen, the markers of each figure represent the average error of every individual residual in the first to fourth stories. The anticipated responses are evaluated by implementing the average values of the structural responses of each behavioral model. Because the extremum points contain valuable information about the overall behavior of the test frame, in Fig. 20, the error value for the first five extremum points of the displacement response of the fourth story is shown for cases 1–4.

Examining Fig. 18, 19, Fig. 20. reveals that:

- For all models, i.e., model_1 to model_4, and for both recursive algorithms, the G-M-P behavior model contains fewer errors than the BWBN material behavior model owing to the relevancy of the BWBN parameters to each other. This result indicates the importance of

Table 4
The initial estimation variation of the mean vector and covariance matrix of G-M-P behavioral model parameters.

			$E(MPa)$	$F_y(MPa)$	b	$R0$	$CR1$	$CR2$	$K_\theta = N^* \times 6EI/l$	ξ
	Assumed**		2e5	360	0.03	15	0.6	0.15	10	0.02
Beam	$Mean = r_i \times \theta_{Assumed}$	r_i	0.75–1.15	0.85–1.15	0.5–1.5	–	0.8–1.5	–	0.75–1.5	0.5–2.0
	Covariance(p_i)	p_i	0.2–0.4	0.2–0.4	0.2–0.4	–	0.2–0.4	–	0.2–0.4	0.2–0.4
Column	$Mean = r_i \times \theta_{Assumed}$	r_i	0.8–1.15	0.75–1.15	0.5–1.5	–	0.75–1.5	–	0.75–1.5	0.5–2.0
	Covariance(p_i)	p_i	0.25–0.4	0.2–0.4	0.25–0.4	–	0.25–0.4	–	0.25–0.4	0.25–0.4

*The N is considered as a variable.
** Assumed vector is considered as baseline.

Table 5
The initial estimation variation of mean vector and covariance matrix of BWBN behavioral model parameters.

			α	K_0	n	δ_ν	δ_η	γ	A_0	δ_A	$K_\theta = N^* \times 6EI/l$	ξ.
Assumed**			0.6	2.5e5	1.0	0.2	0.2	300	1.0	0.2	10	0.02
Beam	$Mean = r_i \times \theta_{Assumed}$	r_i	0.5–2.5	0.75–1.25	0.5–2.0	0.6–2.5	0.6–2.5	0.3–1.5	0.7–1.2	0.6–2.5	0.7–1.5	0.5–2.5
	Covariance(p_i)	p_i	0.15–0.5	0.25–0.5	0.10–0.5	0.25–0.5	0.25–0.5	0.15–0.5	0.3–0.5	0.25–0.5	0.2–0.5	0.2–0.5
Column	$Mean = r_i \times \theta_{Assumed}$	r_i	0.5–2.0	0.8–1.2	0.6–2.5	0.6–2.5	0.6–2.5	0.3–1.5	0.7–1.2	0.6–2.5	0.75–1.5	0.75–2.5
	Covariance(p_i)	p_i	0.25–0.5	0.25–0.5	0.2–0.5	0.25–0.5	0.25–0.5	0.15–0.5	0.3–0.5	0.25–0.5	0.25–0.5	0.25–0.5

*The N is considered as a variable.
** Assumed vector is considered as baseline.

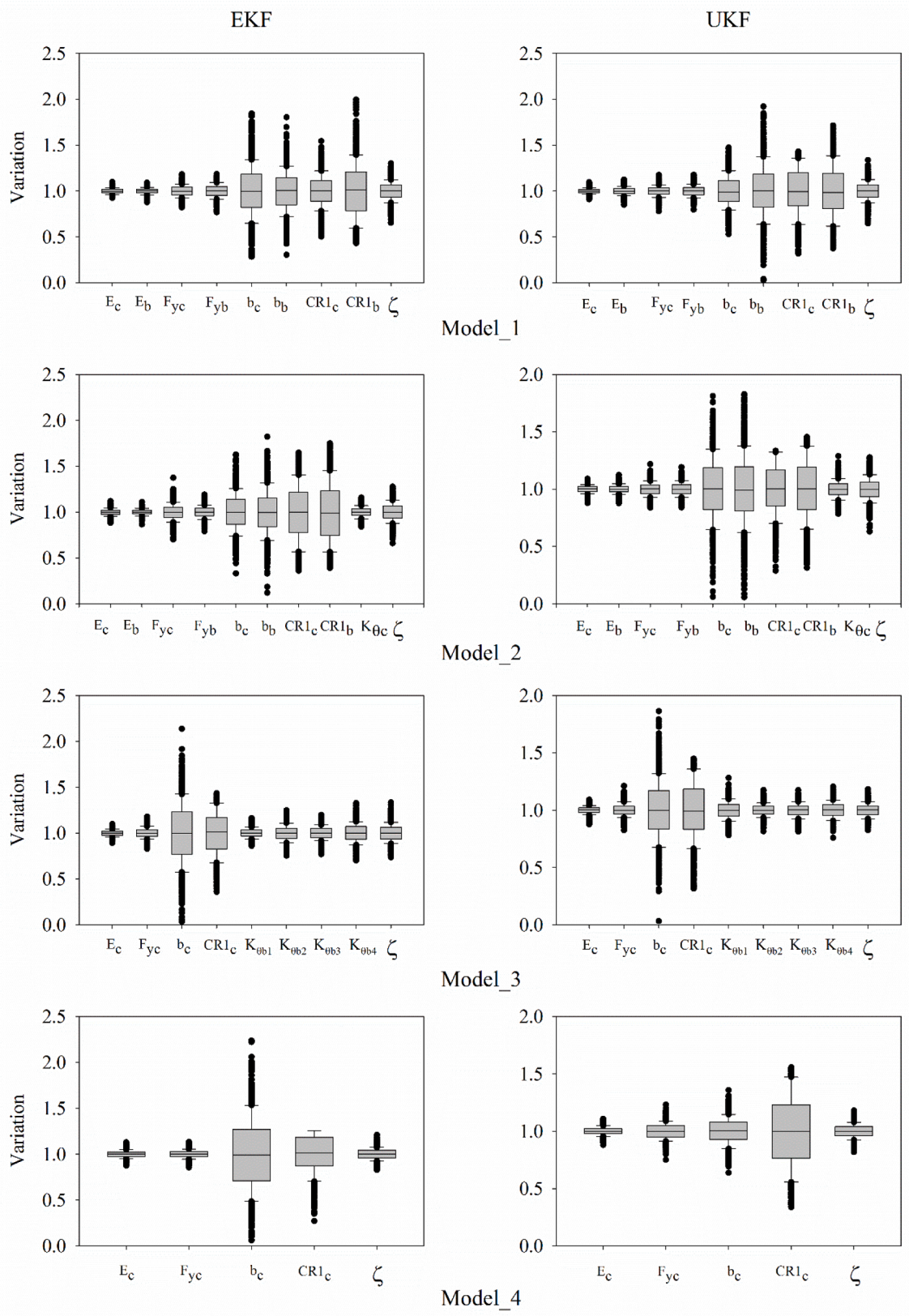

Fig. 12. Parameters variation for G-M-P behavioral model for EKF and UKF algorithms.

selecting appropriate material behavior during calibration. Despite using various initial values of material behavior parameters and their covariance and different combinations of structural responses, employing inappropriate material behavior parameters leads to structural responses with various errors. Although the measured noises result in several errors during the calibration of models, its effect is insignificant compared to the modeling errors.

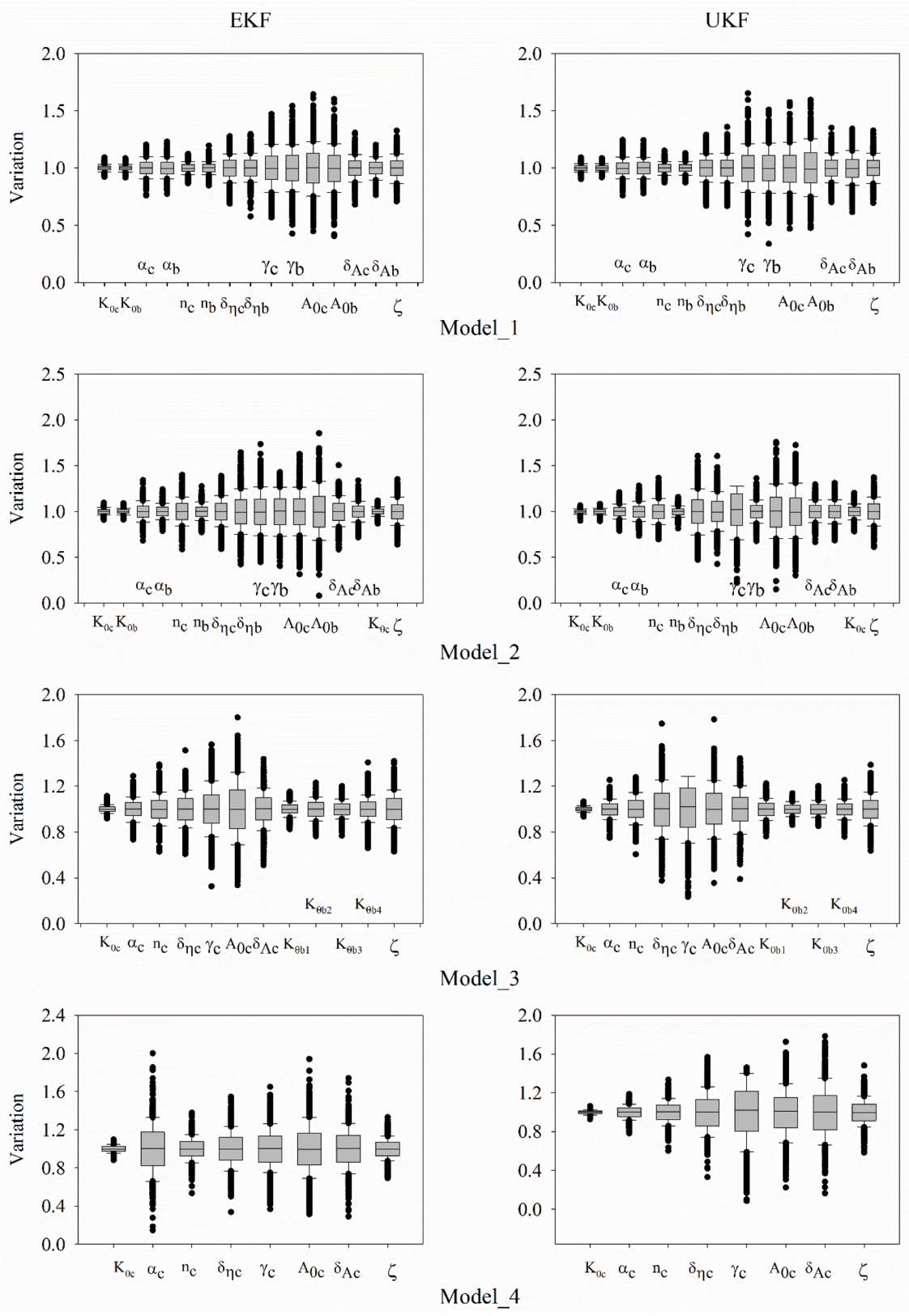

Fig. 13. Parameters variation for the BWBN behavioral model for EKF and UKF algorithms.

- The errors of Model_1 and Model_2 are less than those of Model_3 and Model_4 for all cases. Also, the acceleration responses and the combination of the acceleration and displacement responses of all stories are employed for the EKF and UKF algorithms. This point highlights the effect of modeling assumptions on the accuracy of the calibrated models. Moreover, as expected, provided that the modeling assumptions, including the boundary conditions and constraints, are incorrectly established, the structural model may not be authentically calibrated when using all structural responses.

Table 6
The statistical values obtained for the G-M-P behavioral model parameters.

Model_1

		$E_c(MPa)$	E_b	$F_{yc}(MPa)$	F_{yb}	b_c	b_b	$CR1_c$	$CR1_b$	ξ
EKF	Min	1.85E+05	1.76E+05	295.9	277.0	0.008	0.009	0.30	0.26	0.013
	Max	2.20E+05	2.18E+05	425.9	427.0	0.055	0.054	0.93	1.20	0.026
	Mean	2.03E+05	1.98E+05	362.4	350.1	0.031	0.032	0.62	0.72	0.0196
	STD	5.81E+03	6.38E+03	21.21	25.75	0.008	0.007	0.10	0.18	0.002
UKF	Min	1.82E+05	1.70E+05	280.6	287.4	0.016	0.001	0.19	0.22	0.013
	Max	2.19E+05	2.25E+05	423.0	423.7	0.044	0.058	0.86	1.03	0.027
	Mean	2.01E+05	1.98E+05	351.5	354.5	0.030	0.029	0.52	0.63	0.0202
	STD	5.12E+03	8.44E+03	19.56	20.67	0.005	0.008	0.15	0.17	0.002

Model_2

		$E_c(MPa)$	E_b	$F_{yc}(MPa)$	F_{yb}	b_c	b_b	$CR1_c$	$CR1_b$	K_{0c}	ξ
EKF	Min	1.77E+05	1.73E+05	252.5	284.8	0.010	0.004	0.22	0.23	8.40	0.013
	Max	2.24E+05	2.22E+05	494.8	428.6	0.049	0.055	0.99	1.05	11.58	0.026
	Mean	2.00E+05	1.98E+05	372.2	353.8	0.029	0.030	0.60	0.64	9.96	0.0194
	STD	7.02E+03	6.16E+03	31.6	22.1	0.006	0.007	0.18	0.20	0.53	0.002
UKF	Min	1.76E+05	1.75E+05	301.9	302.8	0.002	0.002	0.17	0.19	7.85	0.013
	Max	2.18E+05	2.25E+05	438.7	429.0	0.054	0.055	0.80	0.87	12.88	0.026
	Mean	1.97E+05	2.01E+05	372.7	366.9	0.027	0.028	0.48	0.54	10.32	0.0225
	STD	6.17E+03	6.93E+03	19.6	20.2	0.008	0.009	0.13	0.16	0.72	0.002

Model_3

		$E_c(MPa)$	$F_{yc}(MPa)$	b_c	$CR1_c$	K_{0b1}	K_{0b2}	K_{0b3}	K_{0b4}	ξ
EKF	Min	1.78E+05	298.0	0.001	0.22	8.61	7.53	7.70	7.00	0.015
	Max	2.19E+05	424.1	0.064	0.86	11.60	12.47	11.97	13.26	0.027
	Mean	1.99E+05	360.8	0.032	0.54	10.12	9.98	9.84	10.11	0.0210
	STD	6.61E+03	20.1	0.010	0.15	0.51	0.82	0.69	1.00	0.002
UKF	Min	1.75E+05	296.8	0.001	0.19	7.80	8.15	8.13	7.60	0.017
	Max	2.18E+05	435.7	0.056	0.87	12.82	11.76	11.73	12.04	0.024
	Mean	1.97E+05	367.4	0.030	0.53	10.31	9.97	9.94	9.87	0.0205
	STD	6.35E+03	19.0	0.008	0.15	0.75	0.50	0.57	0.70	0.001

Model_4

		$E_c(MPa)$	$F_{yc}(MPa)$	b_c	$CR1_c$	ξ
EKF	Min	1.75E+05	307.5	0.002	0.16	0.017
	Max	2.26E+05	407.7	0.067	0.75	0.024
	Mean	2.01E+05	356.3	0.036	0.46	0.0205
	STD	7.79E+03	15.4	0.012	0.12	0.001
UKF	Min	1.76E+05	270.3	0.019	0.20	0.016
	Max	2.21E+05	443.3	0.041	0.93	0.024
	Mean	1.98E+05	358.1	0.030	0.56	0.0199
	STD	7.09E+03	25.0	0.003	0.19	0.001

- Generally speaking, the value of the errors of the displacement responses of all stories is lower than that of the acceleration responses.
- Combining the displacement and acceleration responses of all stories improves the filters' efficiency in the structural identification methods. The explanation is that considering the combination of the responses decreases the effects of measured noises on the calibration process, which is verified by the results of the work by Chatzi and Smyth [21]. In this respect, conformity is more likely to occur when comparing the calculated responses of Case_2 using the displacement responses of the first and third stories to that of Case_3. The results suggest that the accuracy of the filters in identifying the structural response depends on the type and the location of the recorded responses.
- Comparing Case_4 with Case_3 indicates that no considerable improvement in the structural responses is achieved due to the modeling errors. Besides, adding the displacement responses of different stories may not affect the efficiency of the algorithms.
- Considering the results of previous sections, it is concluded that using the EKF and UKF algorithms for both hysteretic models results in achieving various time-invariant parameters, and slight variations can be found between the results of the EKF and UKF. In this respect, UKF can be considered a superior procedure for identifying nonlinear systems. On the other hand, regarding modeling errors, the UKF and EKF can be comparable in terms of accuracy and filtering quality. It is noteworthy that finding different parameters of the G-M-P material model (e.g., F_y and b) and especially the parameters related to the transitions from the elastic to plastic phase ($CR1$) depends on not only the sufficient nonlinearity of the response but also the number and extension of the hysteretic cycles that the structure undergoes.
- Therefore, since the structure has not experienced sufficient nonlinearity, the accuracy of evaluating these parameters is drastically low. Thus, taking advantage of the capability of the UKF algorithm may not be practical.

Fig. 21 compares the hysteretic response of the structure (i.e., the base shear versus the roof displacement and the anticipated responses of Case_4) for both material behavior models using the EKF and UKF methods. Comparing Fig. 14, 15, 16, Fig. 17. with Fig. 21 highlights that the structural responses in the overall scale (e.g., the hysteretic responses) are less accurate than the displacement and acceleration responses. This difference is due to several simplifications, such as considering the concentrated mass for the FE model rather than the distributed one, discretizing the structures, and incorporating several numerical methods in solving problems.

To further study the results, Fig. 22 shows the time histories of posterior estimates of different parameters of G-M-P material models for Cases 1 and 4. As can be seen, the estimation of the Young Modulus parameter, E, is initiated from the beginning of the analysis, in which the base excitation is applied. Meanwhile, if the displacement responses are affected by these parameters, including the F_y and b, their prediction may be initiated.

Besides, for Case_1, the EKF algorithm has not succeeded in

Table 7
The statistical values obtained for the BWBN behavioral model parameters.

Model_1

		K_{0c}	K_{0b}	α_c	α_b	n_c	n_b	$\delta_{\eta c}$	$\delta_{\eta b}$	γ_c	γ_b	A_{0c}	A_{0b}	δ_{Ac}	δ_{Ab}	ξ
EKF	Min	2.31E+05	2.29E+05	0.46	0.46	0.87	0.85	0.14	0.12	170.5	128.2	0.45	0.41	0.14	0.15	0.014
	Max	2.73E+05	2.71E+05	0.72	0.74	1.12	1.20	0.26	0.26	441.8	462.4	1.64	1.60	0.26	0.24	0.027
	Mean	2.53E+05	2.50E+05	0.59	0.60	0.99	1.03	0.20	0.19	306.7	293.3	1.07	1.00	0.20	0.19	0.0206
	STD	6.42E+03	6.67E+03	0.044	0.045	0.044	0.046	0.020	0.020	47.2	50.1	0.191	0.166	0.019	0.015	0.002
UKF	Min	2.26E+05	2.30E+05	0.46	0.47	0.87	0.87	0.13	0.13	126.5	101.6	0.47	0.48	0.14	0.12	0.014
	Max	2.73E+05	2.72E+05	0.75	0.75	1.15	1.13	0.26	0.27	496.0	452.9	1.58	1.60	0.27	0.27	0.027
	Mean	2.50E+05	2.51E+05	0.60	0.61	1.01	1.00	0.20	0.20	313.3	275.0	1.02	1.02	0.21	0.19	0.0206
	STD	6.83E+03	6.67E+03	0.044	0.044	0.046	0.045	0.020	0.021	49.6	50.1	0.173	0.192	0.020	0.024	0.002

Model_2

		K_{0c}	K_{0b}	α_c	α_b	n_c	n_b	$\delta_{\eta c}$	$\delta_{\eta b}$	γ_c	γ_b	A_{0c}	A_{0b}	δ_{Ac}	δ_{Ab}	$K_{\theta c}$	ξ
EKF	Min	2.27E+05	2.28E+05	0.41	0.47	0.59	0.77	0.12	0.08	134.4	121.8	0.32	0.08	0.12	0.14	8.68	0.013
	Max	2.74E+05	2.72E+05	0.81	0.75	1.40	1.28	0.28	0.33	520.6	429.1	1.63	1.85	0.30	0.27	11.19	0.027
	Mean	2.51E+05	2.50E+05	0.61	0.61	1.00	1.02	0.20	0.21	329.8	272.5	0.98	0.96	0.21	0.20	9.96	0.020
	STD	8.02E+03	7.41E+03	0.054	0.042	0.124	0.076	0.026	0.039	62.0	61.2	0.212	0.245	0.026	0.018	0.421	0.002
UKF	Min	2.25E+05	2.24E+05	0.47	0.44	0.70	0.82	0.09	0.09	66.6	203.4	0.15	0.30	0.13	0.14	7.84	0.012
	Max	2.67E+05	2.71E+05	0.73	0.77	1.37	1.16	0.32	0.32	382.8	408.9	1.76	1.73	0.26	0.26	12.03	0.027
	Mean	2.46E+05	2.48E+05	0.60	0.60	1.05	0.99	0.20	0.20	225.1	305.9	0.95	1.00	0.20	0.20	9.92	0.0194
	STD	5.64E+03	7.57E+03	0.040	0.051	0.109	0.049	0.039	0.033	66.0	29.7	0.235	0.228	0.020	0.020	0.689	0.002

Model_3

		K_{0c}	α_c	n_c	$\delta_{\eta c}$	γ_c	A_{0c}	δ_{Ac}	$K_{\theta b1}$	$K_{\theta b2}$	$K_{\theta b3}$	$K_{\theta b4}$	ξ
EKF	Min	2.30E+05	0.44	0.63	0.12	97.6	0.34	0.10	8.24	7.62	7.68	6.59	0.013
	Max	2.79E+05	0.77	1.39	0.30	469.5	1.80	0.29	11.52	12.31	12.01	14.08	0.028
	Mean	2.55E+05	0.60	1.03	0.21	284.8	1.066	0.193	9.90	10.05	9.83	10.27	0.0204
	STD	7.86E+03	0.052	0.116	0.026	56.9	0.243	0.029	0.54	0.82	0.69	0.97	0.003
UKF	Min	2.33E+05	0.45	0.61	0.07	70.0	0.35	0.08	7.61	8.62	8.52	7.58	0.013
	Max	2.67E+05	0.75	1.28	0.35	385.3	1.78	0.29	12.25	11.38	12.03	12.53	0.028
	Mean	2.50E+05	0.60	0.95	0.21	228.3	1.076	0.183	10.00	10.00	10.21	10.02	0.0206
	STD	5.64E+03	0.044	0.109	0.040	65.7	0.200	0.03	0.75	0.50	0.57	0.71	0.002

Model_4

		K_{0c}	α_c	n_c	$\delta_{\eta c}$	γ_c	A_{0c}	δ_{Ac}	ξ
EKF	Min	2.21E+05	0.09	0.53	0.07	110.5	0.31	0.06	0.014
	Max	2.74E+05	1.20	1.38	0.31	495.0	1.94	0.35	0.027
	Mean	2.47E+05	0.65	0.96	0.19	302.8	1.15	0.20	0.0206
	STD	8.88E+03	0.155	0.115	0.036	60.4	0.250	0.041	0.002
UKF	Min	2.32E+05	0.47	0.60	0.07	25.3	0.22	0.03	0.012
	Max	2.66E+05	0.71	1.34	0.31	438.5	1.73	0.36	0.030
	Mean	2.49E+05	0.59	0.97	0.19	228.7	0.99	0.19	0.0211
	STD	5.26E+03	0.039	0.11	0.039	88.6	0.233	0.053	0.003

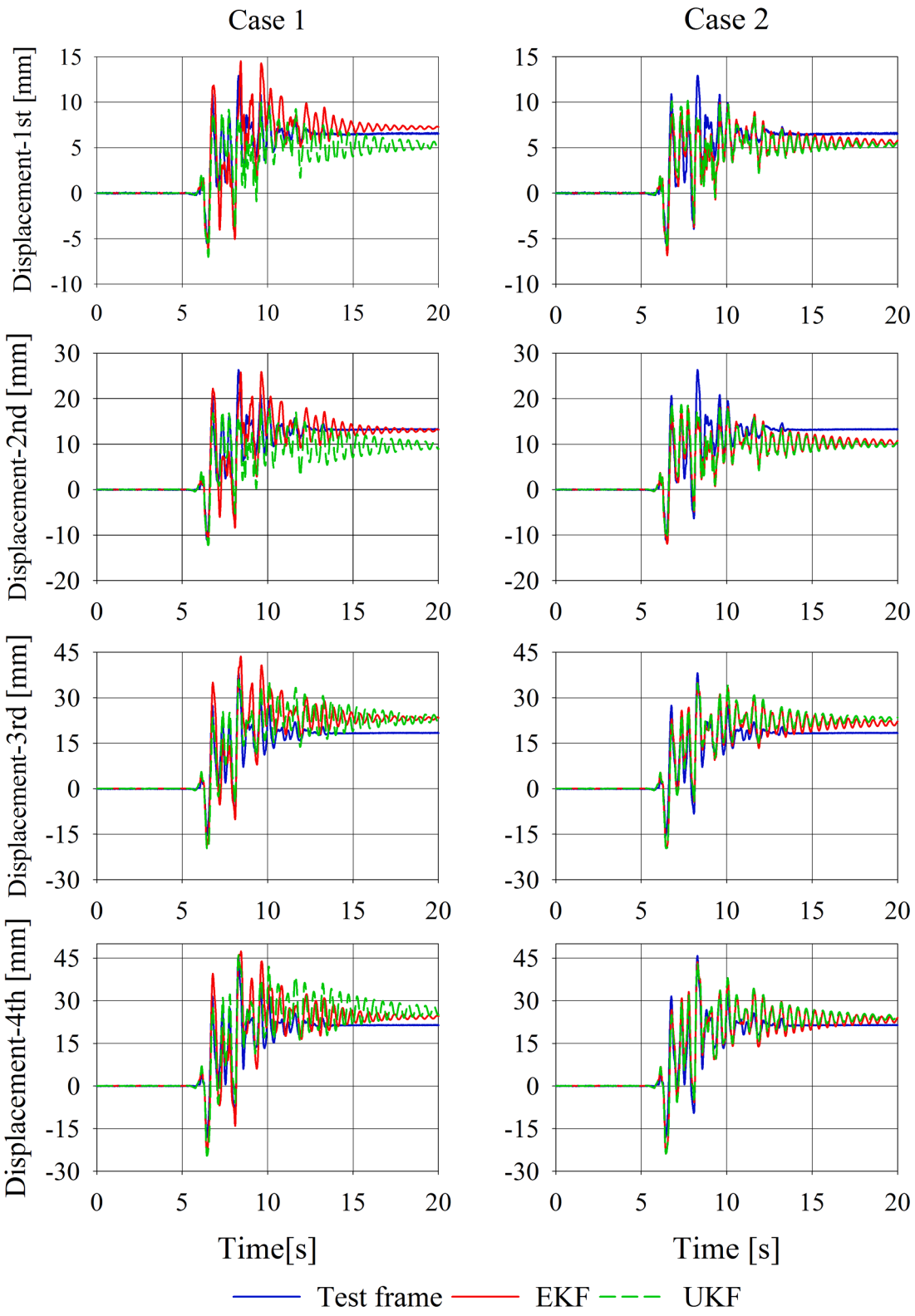

Fig. 14. Comparison of the FE predicted displacement response and the test frame inferred for two Cases(Case_1 and Case_2) for G-M-P material model.

estimating the value of the strain hardening parameter, even though the UKF algorithm shows sensitivity to this parameter. One the other hand, increasing the number of inputs in Case_4, both algorithms become sensitive to all parameters.

6.2. State estimation results under CLE and CLEF

Since the EKF method relies on linearization to propagate the mean and covariance of the estimation error, even though it is one of the most widely used state estimation methods, it may not perform well in dealing with systems with severe nonlinearity. In fact, the main concern with

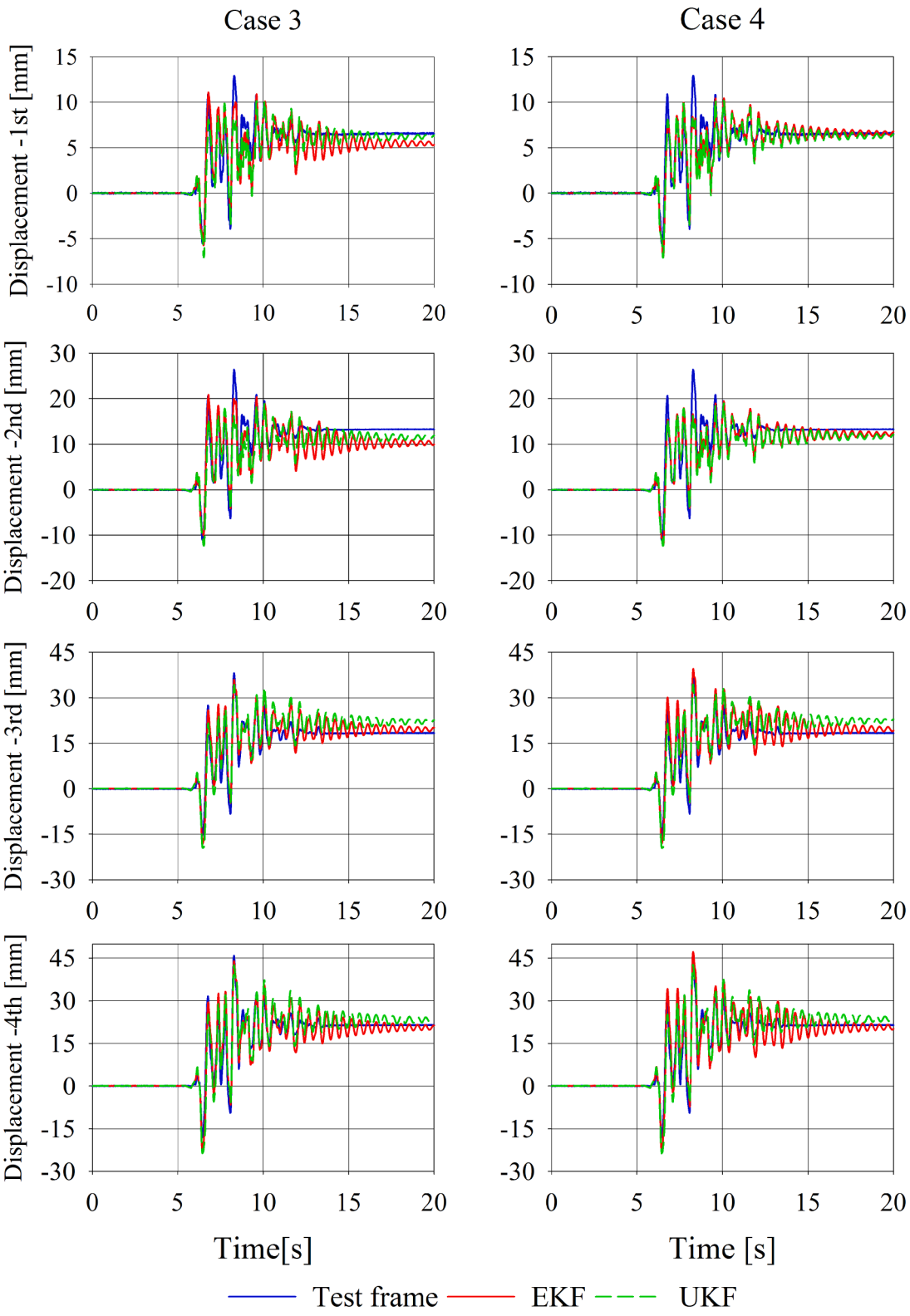

Fig. 15. Comparison of the FE predicted displacement response and the test frame inferred for two Cases(Case_3 and Case_4) for G-M-P material model.

nonlinear systems is the transformation of the PDF through the nonlinear system. The EKF method assumes that a linearized adaptation of means and covariances is approximately equal to the true nonlinear transformation.

The results of the last section showed that under the DLE, this approximation could lead to relatively accurate results. Therefore, in this section, for higher-intensity earthquakes (CLE and CLEF) where the structure undergoes more severe nonlinearity, the estimation ability of this type is compared with that of the UKF method, which takes into account higher-order approximations. For CLE and CLEF earthquakes, both EKF and UKF algorithms were repeated 100 times for the first and second models with the G-M-P material model with different initial

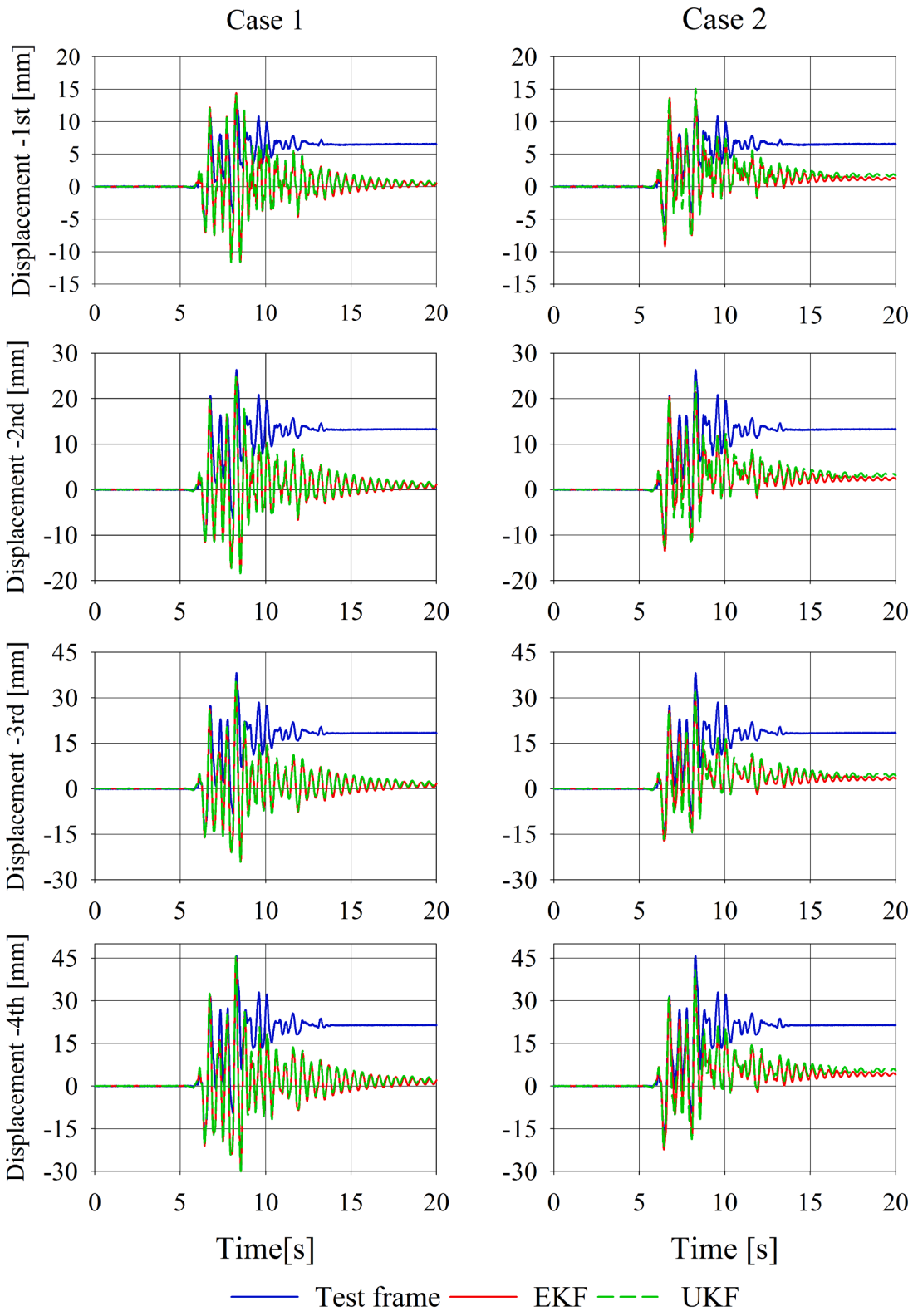

Fig. 16. Comparison of the FE predicted displacement response and the test frame inferred for two Cases (Caee_1 and Case_2) for the BWBN behavioral model.

conditions and various state estimation covariance assumptions. The errors of displacement and acceleration responses of different levels of the structure for both ground motion levels are shown in Fig. 23 and Fig. 24, respectively.

Examining Fig. 23 and Fig. 24 indicates that:

- No numerical convergence problems appear during the incremental integration of the nonlinear equations in these two algorithms, despite the significant nonlinearity of the test structure.
- As expected, with the increase in the earthquake's intensity, the expected growth in the input energy to the structure increases; meanwhile, with the further development and intensification of the

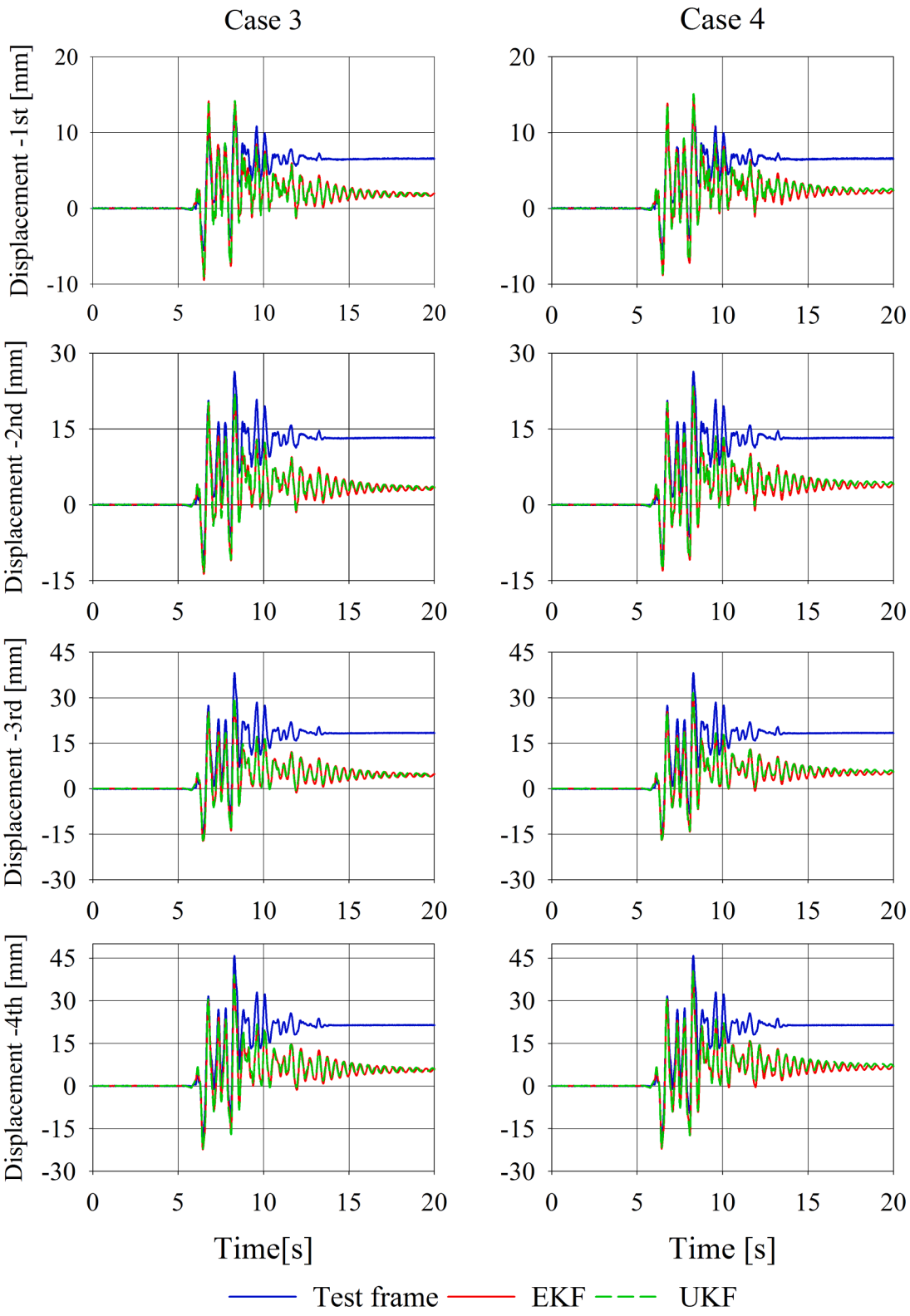

Fig. 17. Comparison of the FE predicted displacement response and the test frame inferred for two Cases (Caee_3 and Case_4) for the BWBN behavioral model.

nonlinearity in the structure, the estimation error of the algorithms increases. Although some of this error is due to the cumulative errors of lower-level earthquakes, a large part is also related to linearization and the use of sigma points in EKF and UKF algorithms, respectively. The error for the EKF algorithm will increase much higher than the UKF.

- Like the results obtained in the earlier section, fusing the acceleration and displacement responses of all levels of the structure has caused the lowest estimation error for both algorithms.

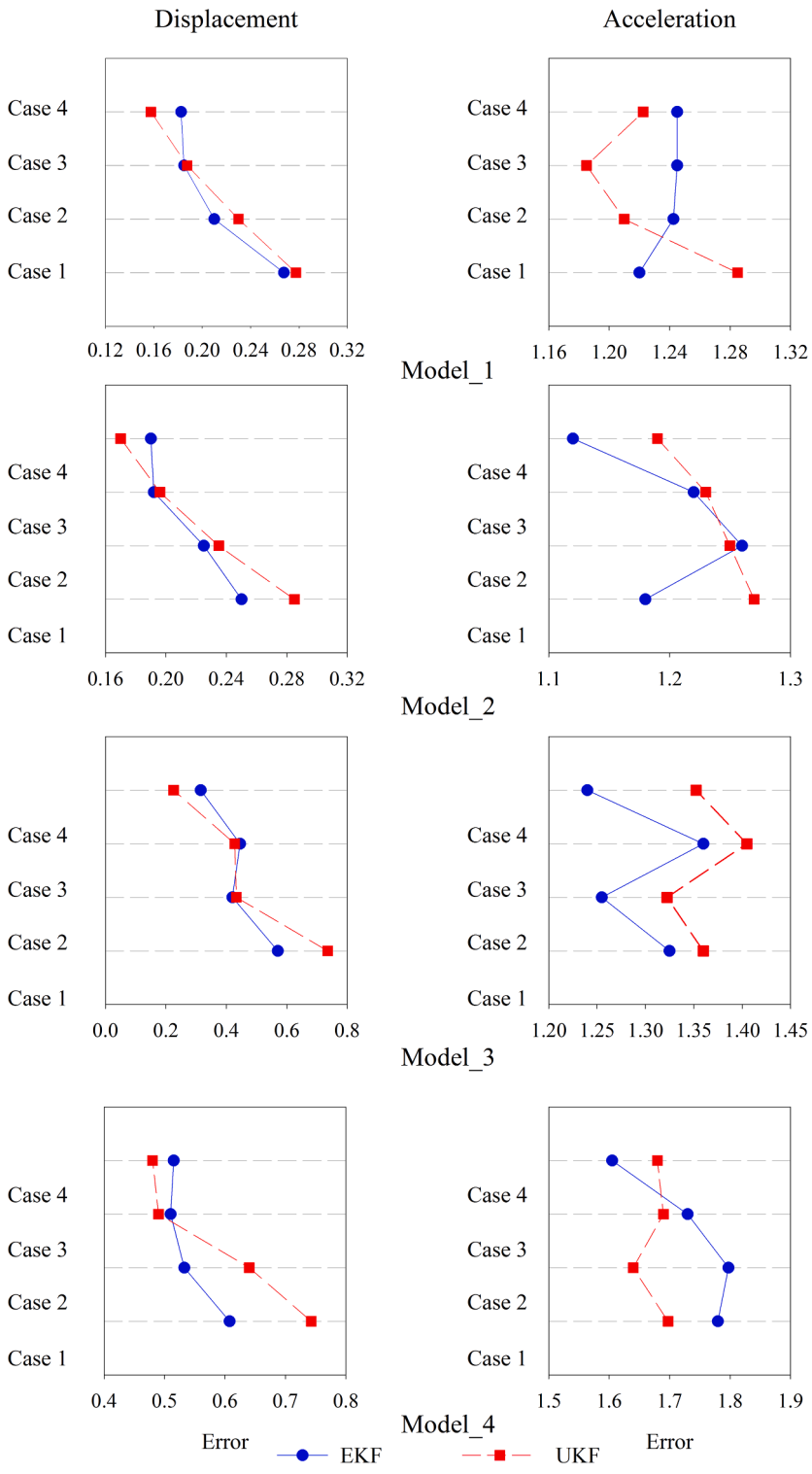

Fig. 18. The error metrics of the structural responses with G-M-P hysteretic model through the EKF and UKF algorithms.

6.3. Information entropy results

To investigate the effects of the second and fourth story responses on improving the calibration and decreasing the errors, the information entropy measure (s/s_0) can be employed according to Eq. (33). In this section, the value of the Young Modulus of different sub-structures is considered an unknown parameter in the system identification process. As highlighted previously, the value of the Young Modulus can considerably affect the structural responses compared to other parameters. Therefore, in this case, two uncertain parameters are considered. Also, measuring the rotational responses of different degrees of freedom of the structure seems almost impossible. However, even if possible, it accompanies difficulty and high costs. Hence, the translational responses of four structural levels under the ambient (white noise), impulsive, and low amplitude vibrations were accumulated and used in the system identification process.

The main reason for employing different excitations is to investigate the effects of different structural inputs on the location of sensors. As

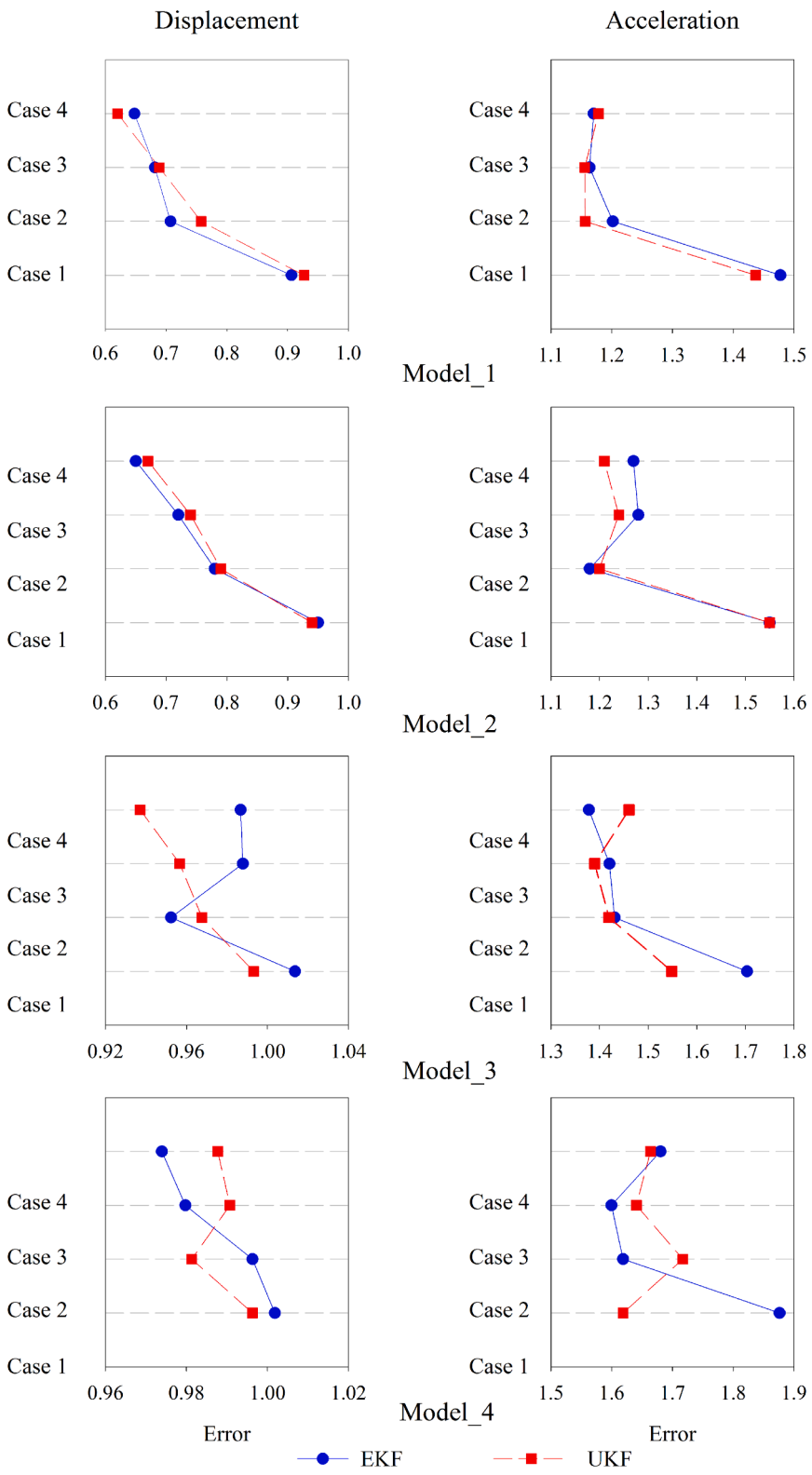

Fig. 19. The error metrics of the structural responses with BWBN hysteretic model through the EKF and UKF algorithms.

stated previously, three different types of excitations were considered, including white noise excitation, excitations below 20% of the earthquake record applied to the structure through the shaking table, and excitations due to the impact loading. It is of note that the impact loads have the potential to excite all modes of vibrations of a structure and capture the effects of higher modes. Consequently, despite the low number of structural floors, this type of vibration can determine the sensor's appropriate location due to considering the effects of higher modes.

Regarding the low impact of the participation of higher modes on the structural responses and the high noise-to-signal ratio of these modes, their effects may not be sharp. Therefore, the impact of these modes was

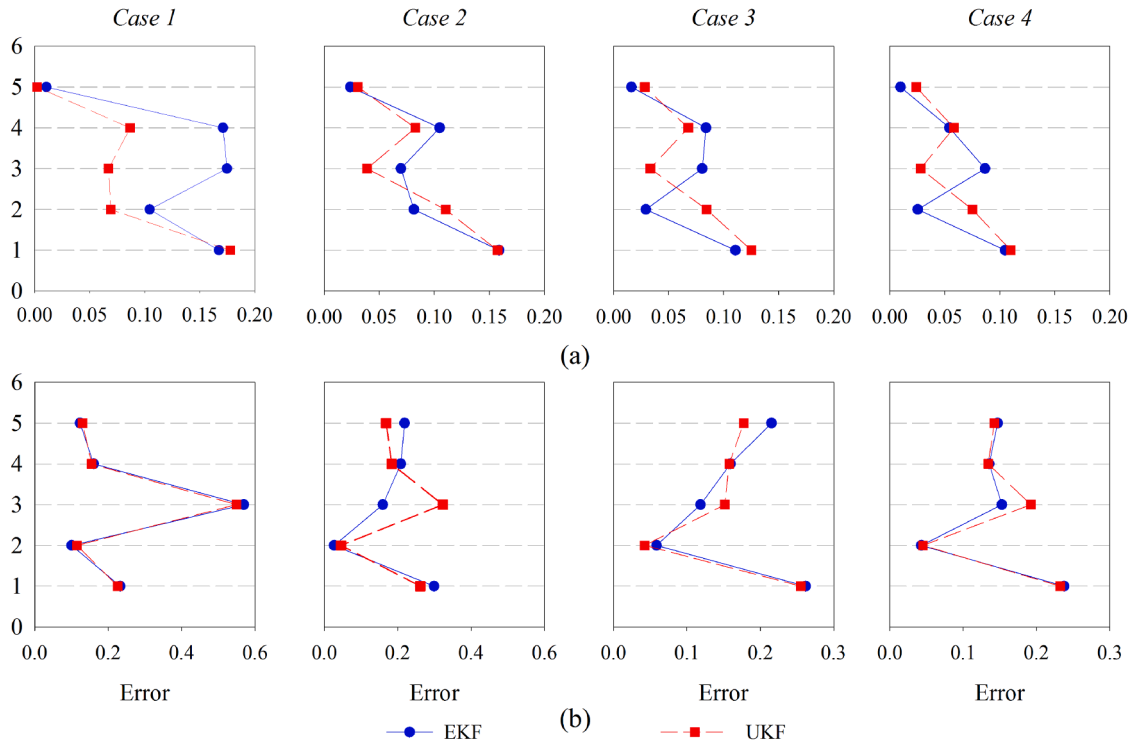

Fig. 20. The error metrics of first five extremum points of the displacement response of the fourth story, (a) G-M-P material model, and (b) BWBN material model.

investigated through impact excitation in the following. Different possible cases can be considered to determine the best location for the placement of sensors, e.g., the placement of sensors on an individual level, two, three, and four different levels of the structure. In fact, for the mentioned cases, 4, 6, 4, and 1 possible locations of sensors and 15 possible locations on the structure can be considered for different excitations, respectively. The value of the IEM ratio (s/s_0) for different excitation cases are summarized in Table 8.

Comparing the results in Table 8 leads to the following conclusions:

- High dispersion of the values of the IEM ratio, along with their mean and standard deviations, can be noticed for every excitation applied to the structure. This observation highlights the importance of considering the location of the sensors for model updating and identification of structures with a low number of stories and limited DOFs.
- According to Table 8, differences can be noticed in the results under different input excitations, suggesting the significance of the type of excitation applied to the structure and its characteristics, including the frequency range, amplitude, and time duration for the structural system identification.
- The lower the value of the IEM ratio (s/s_0), the lower the uncertainties associated with the identification process and the optimal placement of sensors. Hence, using the impact loading excitations results in lower uncertainties. Moreover, employing sensors on an individual level, two or three different levels of the structure results in a noticeable reduction of the IEM ratio for this excitation type.
- In the case of using only an individual sensor on each level of the structure, the dispersion of the IEM ratio is relatively high. According to Table 8, the IEM ratio of the fourth story has the lowest amount for different loading cases. Moreover, the second story is the next in terms of the value of this ratio. However, the IEM ratio shows that the third and first floors are the worst locations for sensing under-shock loading vibrations. White noise and 20% of earthquake excitations for the first and third stories contain nearly identical responses.
- Analyzing the results of two sensors reveals that using the responses of the second and fourth floors improves the responses and reduces the uncertainties compared to the responses of other levels. In this regard, the sensors located on the second and fourth floors by themselves result in an enhanced response compared to other floors, and simultaneous use of the responses of the second and fourth floors causes a low level of uncertainty. Nevertheless, concurrently applying sensors with acceptable responses does not necessarily yield satisfactory results. This simple negation works well for the first and third floors.
- Comparing the results of cases 9 and 11 of Table 8 (sensors located on the second and fourth floors and those located on the first to third floors, respectively) indicates that the structural identification with fewer sensors located at the appropriate places results in a more accurate identification compared to more number of sensors located at the improper locations. The importance of this issue can be considered in identifying the structures with high DOFs, wherein a limited response of DOFs is allowed.

Overall, it is concluded that the best locations for the placement of sensors can be considered as a function of the number of sensors located on the structure, the structural parameterization scheme, and the input excitations. Moreover, using more sensors in improper locations does not enhance the responses.

To investigate this issue further, Fig. 25 represents the two-sided spectral density for different stories in the 1 to 10 Hz frequency range. The mode shapes and frequency of the two first vibration modes are shown in Fig. 26. As can be seen, the responses reach their highest amount at the frequency of 2.2 Hz, where good agreement is observed between the fundamental mode of the structure both in the experiments and numerical models. For measured responses of the second and fourth floors, sharp peaks can be observed. In contrast, for the first and third floors, the peak points are not as good as the sharp peaks of the second and fourth floors. Moreover, the first and second modes can be identified well, while it is not practical in the case of the third and higher modes. Consequently, it can be concluded that identifying the first two modes of

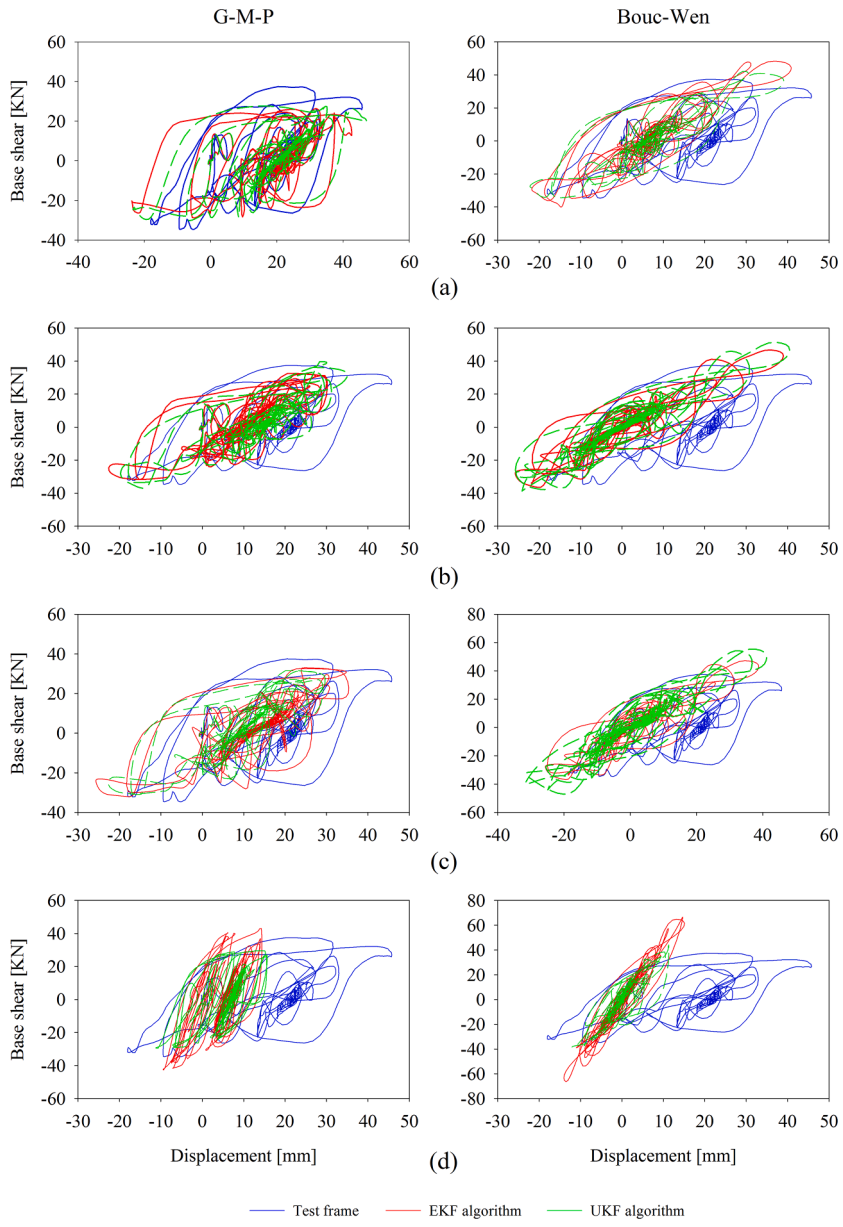

Fig. 21. Comparison between the base shear versus the roof displacement, and the anticipated responses of Case_4 for both behavioral material models using the EKF and UKF methods: (a) Model_1, (b) Model_2, (c) Model_3, and (d) Model_4.

the structure using the responses of the second and fourth floors, rather than those of the first and third floors, improves the findings. Examining Fig. 25 and the results of the entropy-based sensor placement (Table 8) indicates that for the structural system identification, using the confusion of the responses of the second and fourth floors improves the results through the recursive algorithms of UKF and EKF.

7. Conclusions and limitations

This study aimed to identify a 1/8-scale 4-story moment-resisting steel frame under a shaking table test using the recursive, EKF, and UKF algorithms. The test frame was subjected to different excitations, including progressive seismic base excitations, ambient, and impulse excitations. Since the evolution of the FE structural model is a crucial stage in the system identification study, to identify the frame, several uncertainties (i.e., different models of material behavior such as the G-M-P and the BWBN) and several constraints were considered. Besides, the structural responses of different floors were combined for this purpose.

Based on the findings obtained from the identification technique for the structure under the design level earthquake, despite using a linearization technique based on the EKF algorithm, acceptable responses were obtained through this algorithm compared to the advanced UKF algorithm. Due to the correlation of the BWBN material model parameters with each other, employing this model results in high errors compared to the G-M-P material model, even for different initial values of the unknown parameters and covariance matrices of errors. This finding certifies that structural identification of incompatible models using online algorithms may encounter unexpected difficulties.

Moreover, employing the combination of some selected floors' acceleration and displacement responses in the structure identification process improves the calibration process, suggesting that an enhanced calibration process has been obtained using the responses concerning the proper placements of sensors.

To further investigate the optimum placement of sensors, the criterion of the IEM is employed under three different excitations. As

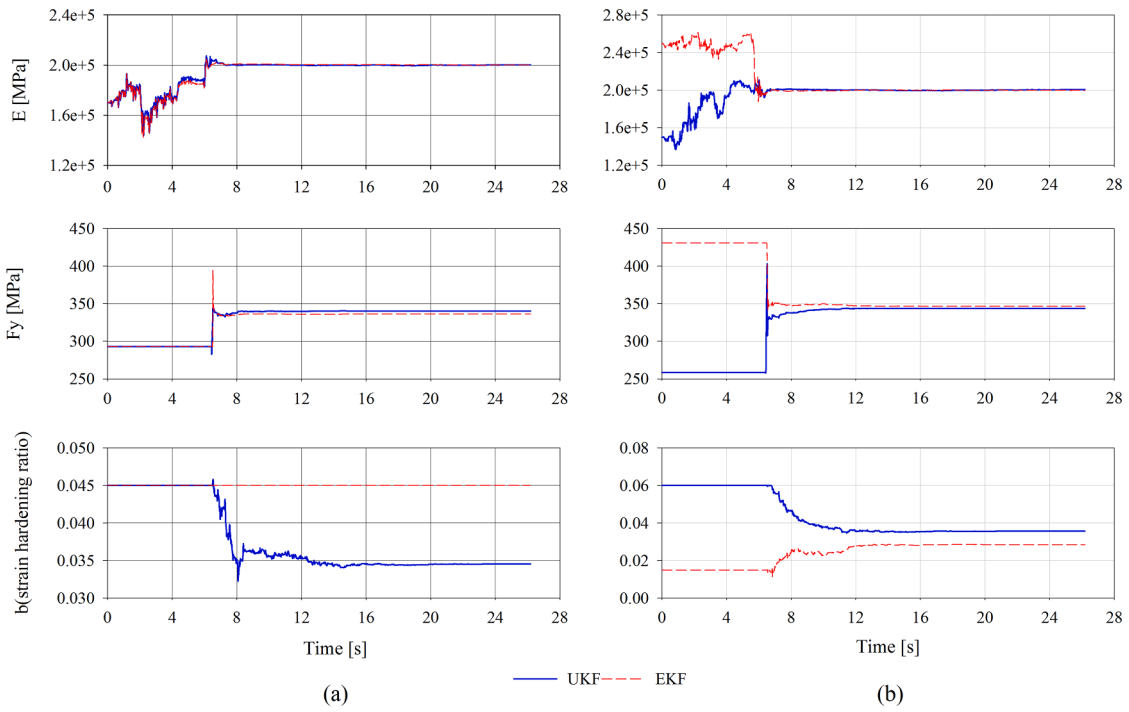

Fig. 22. Time histories of a posteriori of G-M-P material model parameters for EKF and UKF algorithms: (a) for Case_1, and (b) Case_4.

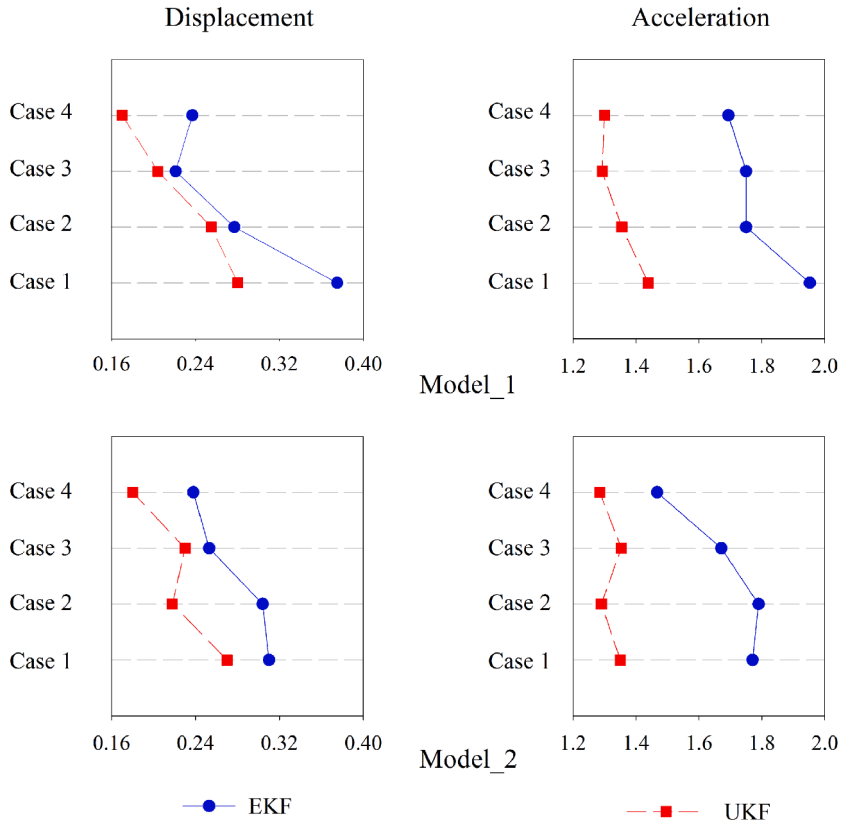

Fig. 23. The error metrics of the structural responses of the G-M-P behavioral model through the EKF and UKF algorithms under CLE.

demonstrated, employing the low-amplitude seismic excitations and impulse excitations results in an identical response, except for the effect of higher modes. This issue has been considered for models under impulse excitations, despite the high noise ratio to signal in their responses.

The results suggest that applying the information entropy results in greater dispersion when using the responses of an individual story or several stories, indicating the importance of using the responses of proper stories in the calibration process. In addition, it proves that using

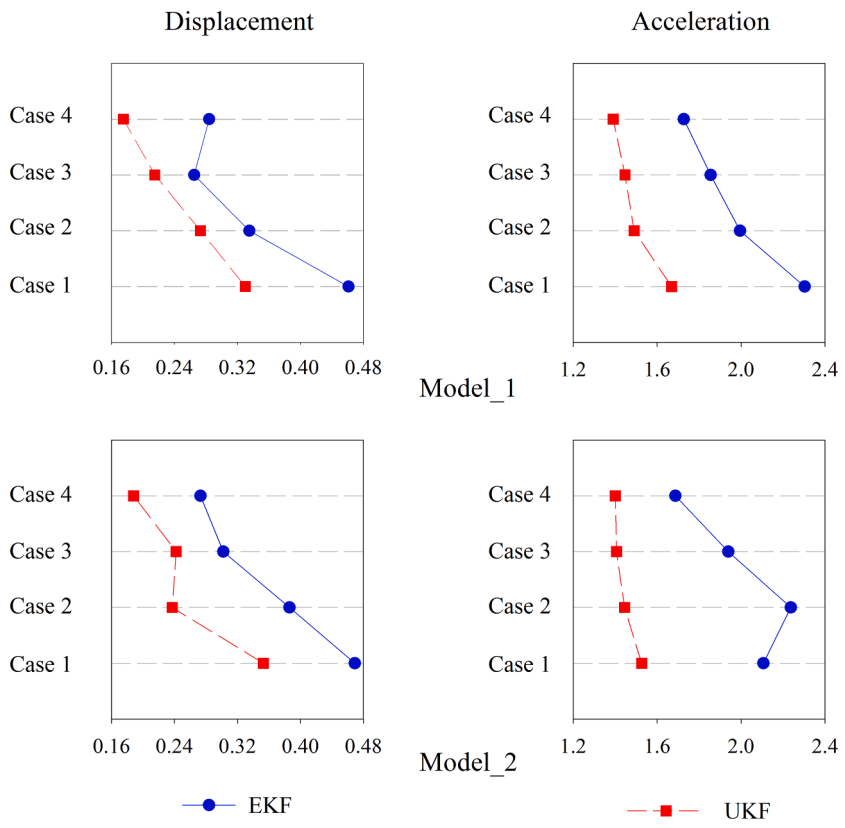

Fig. 24. The error metrics of the structural responses of the G-M-P behavioral model through the EKF and UKF algorithms under CLEF.

Table 8

Information entropy measure $\left(\frac{S}{S_0}\right)$ of different cases of excitation and for different stories responses.

No.	Stories	Ex._case1(White noise)	Ex._case2 (Impulsive)	Ex._case3(Base excitation)
1	1	11.4	10.7	11.2
2	2	7.4	6.75	6.9
3	3	7.15	7.45	7.05
4	4	5.2	4.5	4.9
5	1,2	6.1	5.45	5.25
6	1,3	6.2	5.13	5.9
7	1,4	3.9	3.9	3.75
8	2,3	4.11	4.25	4.42
9	2,4	2.05	1.85	1.9
10	3,4	2.36	1.87	1.95
11	1,2,3	2.25	2.35	2.42
12	1,2,4	1.9	1.4	1.45
13	1,3,4	2.1	1.52	1.7
14	2,3,4	1.35	1.15	1.22
15	1,2,3,4	1	1	1
Mean		4.30	3.95	4.07
STD		2.92	2.80	2.87

fewer sensors positioned optimally leads to improved results compared to using more sensors in improper places. Furthermore, the results agree well with identifying the structure using the two aforementioned recursive algorithms.

However, EKF and UKF techniques often present the disadvantage of demanding high simulation times to update the procedure, especially when dealing with complicated structures. As mentioned before, the primary idea of the EKF algorithm is linearizing the nonlinear function locally by calculating response sensitivities, which need the execution of the FE model for each unknown parameter at each time step. Similarly, the UKF algorithm must run the FE model once for each sigma point at each time step. Another expected drawback of conventional KF-based approaches is that the recursive process may become numerically unstable, especially when the amount of system noise and measurement noise is high. Besides, various uncertainties and modeling errors – e.g., the nonstructural components (infill walls) and systems (architectural layouts) – have not been studied in numerical modeling. Hence, developing new KF-based filters with the minimum number of SPs without nonsingular estimation is necessary for saving time.

Author statement

Mehrdad Ebrahimi, Elnaz Nobahar, Reza Karami Mohammadi, Ehsan Noroozinejad Farsangi, Mohammad Noori & Shaofan Li contributed to the conceptualization, supervision and management of the project. The modeling, analyses and simulations were carried out by Mehrdad Ebrahimi and Elnaz Nobahar. Mehrdad Ebrahimi, Elnaz Nobahar, Reza Karami Mohammadi, Ehsan Noroozinejad Farsangi, Mohammad Noori & Shaofan Li have contributed to data analysis, illustration, organize, read, review, and approve the original draft. All authors have contributed to writing - review & editing of the final submitted version.

CRediT authorship contribution statement

Mehrdad Ebrahimi: Writing – review & editing, Writing – original draft, Visualization, Validation, Supervision, Methodology, Investigation, Formal analysis, Data curation, Conceptualization. **Elnaz Nobahar:** Writing – review & editing, Writing – original draft, Visualization, Validation, Software, Methodology, Investigation, Formal analysis, Data curation, Conceptualization. **Reza Karami Mohammadi:** Writing – review & editing, Writing – original draft, Validation, Supervision, Project administration, Methodology, Investigation, Conceptualization. **Ehsan Noroozinejad Farsangi:** Writing – review & editing, Writing – original

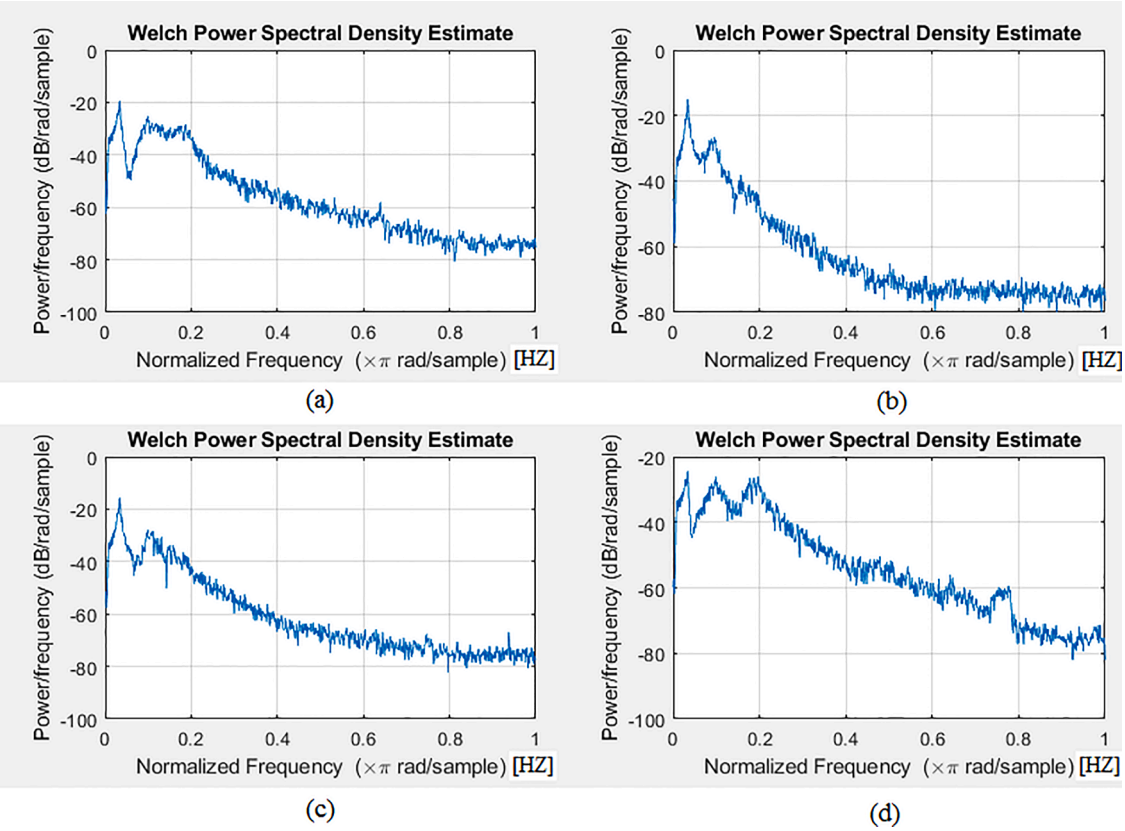

Fig. 25. Spectral densities of acceleration data verus normalized frequency: (a) spectral density for first story, (b) spectral density for second story, (c) spectral density for third story, and (d) spectral density for fourth story.

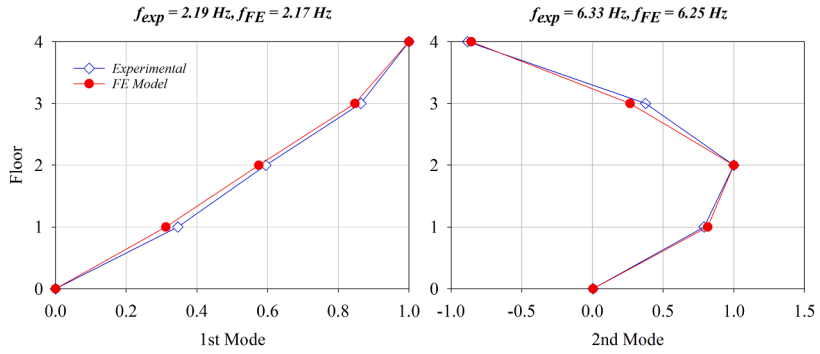

Fig. 26. Mode shapes and frequency of vibration of the test frame.

draft, Validation, Supervision, Project administration, Methodology, Conceptualization. **Mohammad Noori:** Writing – review & editing, Writing – original draft, Validation, Supervision, Project administration, Methodology, Conceptualization. **Shaofan Li:** Writing – review & editing, Writing – original draft, Validation, Supervision, Project administration, Methodology, Conceptualization.

Declaration of Competing Interest

The authors declare that they have no known competing financial interests or personal relationships that could have appeared to influence the work reported in this paper.

Data availability

Data will be made available on request.

References

[1] Hajirasouliha I, Pilakoutas K, Mohammadi RK. Effects of uncertainties on seismic behaviour of optimum designed braced steel frames. Steel and Composite. Structures 2016;20(2):317–35. https://doi.org/10.12989/scs.2016.20.2.317.
[2] Das S, Saha P, Patro S. Vibration-based damage detection techniques used for health monitoring of structures: a review. JCSHM 2016;6(3):477–507.
[3] Nozari A, et al. Effects of variability in ambient vibration data on model updating and damage identification of a 10-story building. Eng Struct 2017;151:540–53.
[4] Behmanesh I, et al. Uncertainty quantification and propagation in dynamic models using ambient vibration measurements, application to a 10-story building. Mech Syst Sig Process 2018;107:502–14.
[5] Ebrahimi M, Mohammadi RKarami. Damage detection of steel moment frames under earthquake excitation. Struct Control Health Monit 2020;27(10):e2599.
[6] Ceroni F, et al. Damage assessment in single-nave churches and analysis of the most recurring mechanisms after the 2016–2017 central Italy earthquakes. Bull Earthquake Eng 2022:1–29.
[7] Kerschen G, et al. Past, present and future of nonlinear system identification in structural dynamics. Mech Syst Sig Process 2006;20(3):505–92.

[8] Astroza R, Alessandri A. Effects of model uncertainty in nonlinear structural finite element model updating by numerical simulation of building structures. Struct Control Health Monit 2019;26(3):e2297.
[9] Gharehbaghi VR, Farsangi EN, Yang TY, Hajirasouliha I. Deterioration and damage identification in building structures using a novel feature selection method. Structures 2021;29:458–70. https://doi.org/10.1016/j.istruc.2020.11.040.
[10] Casapulla C, Maione A. Experimental and analytical investigation on the corner failure in masonry buildings: interaction between rocking-sliding and horizontal flexure. Int J Archit Herit 2020;14(2):208–20. https://doi.org/10.1080/15583058.2018.1529206.
[11] Casapulla C. Local out-of-plane failure modes in traditional block-masonry buildings. In Masonry Construction in Active Seismic Regions; Woodhead Publishing Series in Civil and Structural Engineering; Rupakhety. The Netherlands: R., Gautam, D., Eds.; Elsevier: Amsterdam; 2021. p. 289–322. 10.1016/B978-0-12-821087-1.00001-6; 2021.
[12] Xin Y, et al. Post-earthquake reliability assessment of segmental column structures based on nonlinear model updating. Eng Struct 2023;283:115894.
[13] Pacini BR, et al. Nonlinear finite element model updating, part I: experimental techniques and nonlinear modal model parameter extraction. Dynamics of coupled structures, 4. Springer; 2017. p. 263–74.
[14] Ebrahimi M, Mohammadi RKarami, Sharafi F. The Particle Filter and Extended Kalman Filter methods for the structural system identification considering various uncertainties. J Numer Methods Civil Eng 2020;4(3):42–58.
[15] Celano T, et al. Thermographic investigations and dynamic identification tests for non-destructive structural assessment and enhanced FE modelling of a historical iron-strengthened masonry church. JCSHM 2022:1–24.
[16] Jategaonkar RV. Flight vehicle system identification: a time-domain methodology. American Institute of Aeronautics and Astronautics, Inc; 2015.
[17] Erazo K, Nagarajaiah S. An offline approach for output-only Bayesian identification of stochastic nonlinear systems using unscented Kalman filtering. J Sound Vib 2017;397:222–40.
[18] Chowdhury FN. Input-output modeling of nonlinear systems with time-varying linear models. IEEE Trans Autom Control 2000;45(7):1355–8.
[19] Yang JN, Lin S. Identification of parametric variations of structures based on least squares estimation and adaptive tracking technique. J Eng Mech 2005;131(3):290–8.
[20] Smyth A, et al. Online parametric identification of MDOF nonlinear hysteretic systems. J Eng Mech 1999;125(2):133–42.
[21] Chatzi EN, Smyth AW. The unscented Kalman filter and particle filter methods for nonlinear structural system identification with non-collocated heterogeneous sensing. Struct Control Health Monit 2009;16(1):99–123.
[22] Arulampalam MS, et al. A tutorial on particle filters for online nonlinear/non-Gaussian Bayesian tracking. IEEE Trans Signal Process 2002;50(2):174–88.
[23] Zhang Y, et al. Resilience assessment approach of mechanical structure combining finite element models and dynamic Bayesian networks. Reliab Eng Syst Saf 2021;216:108043.
[24] Cheng K, Lu Z. Adaptive Bayesian support vector regression model for structural reliability analysis. Reliab Eng Syst Saf 2021;206:107286.
[25] Bernal D. Kalman filter damage detection in the presence of changing process and measurement noise. Mech Syst Sig Process 2013;39(1–2):361–71.
[26] Ghanem R, Ferro G. Health monitoring for strongly nonlinear systems using the Ensemble Kalman filter. Struct Control Health Monit 2006;13(1):245–59.
[27] Wei D, Li D, Huang J. Improved force identification with augmented Kalman filter based on the sparse constraint. Mech Syst Sig Process 2022;167:108561.
[28] Erazo K, Moaveni B, Nagarajaiah S. Bayesian seismic strong-motion response and damage estimation with application to a full-scale seven story shear wall structure. Eng Struct 2019;186:146–60.
[29] Huang Y, et al. Sequential sparse Bayesian learning with applications to system identification for damage assessment and recursive reconstruction of image sequences. Comput Meth Appl Mech Eng 2021;373:113545.
[30] Bai G, et al. Prognostics of Lithium-Ion batteries using knowledge-constrained machine learning and Kalman filtering. Reliab Eng Syst Saf 2023;231:108944.
[31] Aswal N, Sen S, Mevel L. Switching Kalman filter for damage estimation in the presence of sensor faults. Mech Syst Sig Process 2022;175:109116.
[32] Huang Jz, et al. Improved Kalman filter damage detection approach based on lp regularization. Struct Control Health Monit 2019;26(10):e2424.
[33] Sen S, Bhattacharya B. Online structural damage identification technique using constrained dual extended Kalman filter. Struct Control Health Monit 2017;24(9):e1961.
[34] Hoshiya M, Saito E. Structural identification by extended Kalman filter. J Eng Mech 1984;110(12):1757–70.
[35] Yang J, Pan S, Huang H. An adaptive extended Kalman filter for structural damage identifications II: unknown inputs. Struct Control Health Monit 2007;14(3):497–521.
[36] Simon D. Optimal state estimation: Kalman, H infinity, and nonlinear approaches. John Wiley & Sons; 2006.
[37] Hartikainen J, Solin A, Särkkä S. Optimal filtering with Kalman filters and smoothers. Department of biomedica engineering and computational sciences. Aalto University School of Science; 2011. 16th August.
[38] Julier S, Uhlmann J, Durrant-Whyte HF. A new method for the nonlinear transformation of means and covariances in filters and estimators. IEEE Trans Autom Control 2000;45(3):477–82.
[39] Julier SJ, Uhlmann JK. Unscented filtering and nonlinear estimation. Proc IEEE 2004;92(3):401–22.
[40] Wan EA, Van Der Merwe R. The unscented Kalman filter for nonlinear estimation. In: Proceedings of the IEEE 2000 Adaptive Systems for Signal Processing, Communications, and Control Symposium (Cat. No. 00EX373). Ieee; 2000.
[41] Wu M, Smyth AW. Application of the unscented Kalman filter for real-time nonlinear structural system identification. Struct Control Health Monit 2007;14(7):971–90.
[42] Baber TT, Noori MN. Random vibration of degrading, pinching systems. J Eng Mech 1985;111(8):1010–26.
[43] Zhao Y, et al. A comparison of three different methods for the identification of hysterically degrading structures using BWBN model. Front Built Environ 2019;4:80.
[44] Jeen-Shang L, Yigong Z. Nonlinear structural identification using extended Kalman filter. Comput Struct 1994;52(4):757–64.
[45] Diaz M, Charbonnel PÉ, Chamoin L. A new Kalman filter approach for structural parameter tracking: application to the monitoring of damaging structures tested on shaking-tables. Mech Syst Sig Process 2023;182:109529.
[46] Wen YK. Method for random vibration of hysteretic systems. J Eng Mech Div 1976;102(2):249–63.
[47] Bouc, R. Forced vibrations of mechanical systems with hysteresis. in Proc. of the Fourth Conference on Nonlinear Oscillations, Prague, 1967. 1967.
[48] Astroza R, Ebrahimian H, Conte JP. Material parameter identification in distributed plasticity FE models of frame-type structures using nonlinear stochastic filtering. J Eng Mech 2015;141(5):04014149.
[49] de Santana Gomes WJ, Beck AT. A conservatism index based on structural reliability and model errors. Reliab Eng Syst Saf 2021;209:107456.
[50] Zhang K, et al. An efficient reliability analysis method for structures with hybrid time-dependent uncertainty. Reliab Eng Syst Saf 2022;228:108794.
[51] Tohme T, Vanslette K, Youcef-Toumi K. Reliable neural networks for regression uncertainty estimation. Reliab Eng Syst Saf 2023;229:108811.
[52] Meng Z, et al. Hybrid uncertainty propagation and reliability analysis using direct probability integral method and exponential convex model. Reliab Eng Syst Saf 2022;228:108803.
[53] Liu X, et al. Mixed uncertainty analysis for dynamic reliability of mechanical structures considering residual strength. Reliab Eng Syst Saf 2021;209:107472.
[54] Mi J, et al. An evidential network-based hierarchical method for system reliability analysis with common cause failures and mixed uncertainties. Reliab Eng Syst Saf 2022;220:108295.
[55] Xu M, et al. Resilience-driven repair sequencing decision under uncertainty for critical infrastructure systems. Reliab Eng Syst Saf 2022;221:108378.
[56] Thapa M, Missoum S. Uncertainty quantification and global sensitivity analysis of composite wind turbine blades. Reliab Eng Syst Saf 2022;222:108354.
[57] Hao P, et al. Stochastic isogeometric buckling analysis of composite shell considering multiple uncertainties. Reliab Eng Syst Saf 2023;230:108912.
[58] Vishwanath BS, Banerjee S. Considering uncertainty in corrosion process to estimate life-cycle seismic vulnerability and risk of aging bridge piers. Reliab Eng Syst Saf 2023;232:109050.
[59] Zheng XW, Li HN, Gardoni P. Hybrid Bayesian-Copula-based risk assessment for tall buildings subject to wind loads considering various uncertainties. Reliab Eng Syst Saf 2023:109100.
[60] Li C, et al. Seismic performance assessment of a sea-crossing cable-stayed bridge system considering soil spatial variability. Reliab Eng Syst Saf 2023;235:109210.
[61] Moaveni B, et al. Uncertainty analysis of system identification results obtained for a seven-story building slice tested on the UCSD-NEES shake table. Struct Control Health Monit 2014;21(4):466–83.
[62] Asgarieh E, et al. Nonlinear model calibration of a shear wall building using time and frequency data features. Mech Syst Sig Process 2017;85:236–51.
[63] Kalman, R.E., A new approach to linear filtering and prediction problems. 1960.
[64] Risken H, Eberly J. The fokker-planck equation, methods of solution and applications. J Optical Soc Am B Optical Phys 1985;2(3):508.
[65] Schei TS. A finite-difference method for linearization in nonlinear estimation algorithms. Automatica 1997;33(11):2053–8.
[66] Tsay J, Cardoso J, Arora J. Nonlinear structural design sensitivity analysis for path dependent problems. Part 2: analytical examples. Comput Meth Appl Mech Eng 1990;81(2):209–28.
[67] Astroza R, Ebrahimian H, Conte JP. Performance comparison of Kalman− based filters for nonlinear structural finite element model updating. J Sound Vib 2019;438:520–42.
[68] Bell BM, Cathey FW. The iterated Kalman filter update as a Gauss-Newton method. IEEE Trans Autom Control 1993;38(2):294–7.
[69] Mei W, Shan G, Wang C. Practical development of the second-order extended Kalman filter for very long range radar tracking. Signal Process 2011;91(5):1240–8.
[70] Bar-Shalom, Y., X.R. Li, and T. Kirubarajan, Estimation with applications to tracking and navigation: theory algorithms and software. 2004: John Wiley & Sons.
[71] Henriksen R. The truncated second-order nonlinear filter revisited. IEEE Trans Autom Control 1982;27(1):247–51.
[72] Uhlmann JK. Dynamic map building and localization: new theoretical foundations. University of Oxford Oxford; 1995.
[73] Julier SJ, Uhlmann JK. Reduced sigma point filters for the propagation of means and covariances through nonlinear transformations. In: Proceedings of the 2002 American Control Conference (IEEE Cat. No. CH37301). IEEE; 2002.
[74] Papakonstantinou KG, Amir M, Warn GP. A Scaled Spherical Simplex Filter (S3F) with a decreased n+ 2 sigma points set size and equivalent 2n+ 1 Unscented Kalman Filter (UKF) accuracy. Mech Syst Sig Process 2022;163:107433.
[75] Haykin SS, Haykin SS. Kalman filtering and neural networks, 284. Wiley Online Library; 2001.

[76] Reuland Y, Lestuzzi P, Smith IF. Data-interpretation methodologies for nonlinear earthquake response predictions of damaged structures. Front Built Environ 2017; 3:43.
[77] Papadimitriou C, Beck JL, Au SK. Entropy-based optimal sensor location for structural model updating. J Vib Control 2000;6(5):781–800.
[78] Rubinstein R. The cross-entropy method for combinatorial and continuous optimization. Methodol Comput Appl Probab 1999;1:127–90.
[79] Katafygiotis LS, Papadimitriou C, Lam HF. A probabilistic approach to structural model updating. Soil Dyn Earthquake Eng 1998;17(7–8):495–507.
[80] Jaynes ET. Where do we stand on maximum entropy?. The maximum entropy formalism. 1979. p. 15.
[81] Papadimitriou C. Optimal sensor placement methodology for parametric identification of structural systems. J Sound Vib 2004;278(4–5):923–47.
[82] Lignos D, Krawinkler H, Whittaker A. Prediction and validation of sidesway collapse of two scale models of a 4-story steel moment frame. Earthquake Eng Struct Dyn 2011;40(7):807–25.
[83] McKenna F. OpenSees: a framework for earthquake engineering simulation. Comput Sci Eng 2011;13(4):58–66.
[84] Taucer F, Spacone E, Filippou FC. A fiber beam-column element for seismic response analysis of reinforced concrete structures, 91. Earthquake Engineering Research Center, College of Engineering, University …; 1991.
[85] Vuillod B, et al. A comparison between Sobol's indices and Shapley's effect for global sensitivity analysis of systems with independent input variables. Reliab Eng Syst Saf 2023;234:109177.
[86] Takeda S, Kitada T. Simple method based on sensitivity coefficient for stochastic uncertainty analysis in probabilistic risk assessment. Reliab Eng Syst Saf 2021;209: 107471.
[87] Nogal M, Nogal A. Sensitivity method for extreme-based engineering problems. Reliab Eng Syst Saf 2021;216:107997.
[88] Xiong Q, et al. Global sensitivity analysis for nuclear reactor LBLOCA with time-dependent outputs. Reliab Eng Syst Saf 2022;221:108337.
[89] Chopra AK. Dynamics of structures. theory and applications to. Earthquake Engineering; 2017.
[90] MATLAB and S.T. release. Natick, Massachusetts, United States: The MathWorks, Inc.; 2015.